(F1)

(18) AFOSR-TR-77-1272

Aeronautical and Astronautical Engineering Department
University of Illinois at Urbana-Champaign

(14) Technical Report AAE-77-15
UILU-Eng-77-0515

(11)

Prepared for

Air Force Office of Scientific Research
Aerospace Sciences Directorate
Bolling Air Force Base, D.C.

(6) DIRECT INITIATION OF DETONATION.

by

(10) Roger A. Strehlow
[redacted]
Harold O. Barthel

(9) Final rpt.
1 Jun 73-31 May 77

Approved for public release; distribution unlimited

Grant No. AFOSR-73-2524
(15)
(11) Sep[redacted] 1977
Final Report
AFOSR-TR
(16) 9711 (17) 02
(19) 62p.

Conditions of Reproduction

AB

UNCLASSIFIED

SECURITY CLASSIFICATION OF THIS PAGE (When Data Entered)

REPORT DOCUMENTATION PAGE		READ INSTRUCTIONS BEFORE COMPLETING FORM
1. REPORT NUMBER AFOSR-TR- 77 - 1272	2. GOVT ACCESSION NO.	3. RECIPIENT'S CATALOG NUMBER
4. TITLE (and Subtitle) DIRECT INITIATION OF DETONATION		5. TYPE OF REPORT & PERIOD COVERED 1 June 1973 - 31 May 1977 FINAL
		6. PERFORMING ORG. REPORT NUMBER
7. AUTHOR(s) Roger A. Strehlow and Harold O. Barthel		8. CONTRACT OR GRANT NUMBER(s) AFOSR 73-2524
9. PERFORMING ORGANIZATION NAME AND ADDRESS UNIVERSITY OF ILLINOIS AT URBANA-CHAMPAIGN AERONAUTICAL AND ASTRONAUTICAL ENGINEERING DEPT URBANA, IL 61801		10. PROGRAM ELEMENT, PROJECT, TASK AREA & WORK UNIT NUMBERS 9711-02 61102F
11. CONTROLLING OFFICE NAME AND ADDRESS AIR FORCE OFFICE OF SCIENTIFIC RESEARCH/NA BLDG 410, BOLLING AIR FORCE BASE, D.C. 20332		12. REPORT DATE September 1977 13. NUMBER OF PAGES 59
14. MONITORING AGENCY NAME & ADDRESS(if different from Controlling Office)		15. SECURITY CLASS. (of this report) UNCLASSIFIED 15a. DECLASSIFICATION/DOWNGRADING SCHEDULE

16. DISTRIBUTION STATEMENT (of this Report)

Approved for public release; distribution unlimited.

17. DISTRIBUTION STATEMENT (of the abstract entered in Block 20, if different from Report)

18. SUPPLEMENTARY NOTES

19. KEY WORDS (Continue on reverse side if necessary and identify by block number)

DETONATION INITIATION
BLAST WAVES

20. ABSTRACT (Continue on reverse side if necessary and identify by block number)

This study is both a theoretical and experimental investigation of the initiation of detonation by non-ideal blast waves. The theoretical portions consisted of two studies: (1) an analytic study of the flow fields associated with heat addition during the initial phases of heat addition to a source region which is chemically reactive, and (2) a study of the initiation of explosions by non-ideal sources using a numerical technique. The analytic portion of this study uncovered many difficulties with the handling of the heat addition in a reactive

DD FORM 1 JAN 73 1473 EDITION OF 1 NOV 65 IS OBSOLETE

UNCLASSIFIED

SECURITY CLASSIFICATION OF THIS PAGE (When Data Entered)

source region. These are discussed extensively in this report. The numerical calculation showed that when the source region was a bursting sphere of high energy density, the total energy in the sphere was the limiting factor for initiation and that when the energy density of the sphere was low the energy density was the limiting factor for initiation. Furthermore, as the energy density dropped the energy required for initiation increased markedly. This agrees quite well in a qualitative sense with experimental observations from spark initiated detonations. The experimental program also consisted of two phases. In one of these, reflected initiation of propylene oxide-nitrogen-oxygen mixtures was studied over the temperature range of about 1000-2500°K. The data were correlated to an Arrhenius temperature dependency and yielded an activation energy of approximately 38,000 cal/gm mole. The other experimental study investigated the effect of inhibitors and promotors on the delayed time to ignition for propane-air mixtures, also using the reflected shock technique.

DIRECT INITIATION OF DETONATION

Grant No. AFOSR 73-2524

Principal Investigators: Roger A. Strehlow and Harold O. Barthel

Statement of Progress:

Theoretically we found that when a non-ideal blast wave and exothermic reaction kinetics are modeled realistically, both the total source energy and the source energy density are important to the direct initiation process. At high energy densities the total energy is limiting, and as the energy density decreases the total energy required increases until at some critical low energy density the energy density itself becomes the limiting factor for initiation. This confirms the experimental observations made by John Lee at McGill University. We have also learned how the non-ideality of a source region influences the structure of a blast wave. Specifically, the blast wave from bursting spheres, the ramp addition of energy, constant velocity centrally ignited spherical flames, and accelerated spherical flames have been studied extensively, and this has yielded the generalization that far field positive impulse is properly scaled by the source energy but that for low power density sources far field overpressure falls below the expected energy scaled value.

Experimentally the initiation kinetics of propylene oxide-nitrogen-oxygen mixtures was studied over the temperature range of 1000-2500°K. These results show the usual Arrhenius dependence on temperature for the ignition delay.

This work has led to three M.S. and two Ph.D. theses, two interim technical reports, four papers in the open literature and seven presentations at meetings and seminars.

DIRECT INITIATION OF DETONATION

ABSTRACT

This study is both a theoretical and experimental investigation of the initiation of detonation by non-ideal blast waves. The theoretical portions consisted of two studies: (1) an analytic study of the flow fields associated with heat addition during the initial phases of heat addition to a source region which is chemically reactive, and (2) a study of the initiation of explosions by non-ideal sources using a numerical technique. The analytic portion of this study uncovered many difficulties with the handling of the heat addition in a reactive source region. These are discussed extensively in this report. The numerical calculation showed that when the source region was a bursting sphere of high energy density, the total energy in the sphere was the limiting factor for initiation and that when the energy density of the sphere was low the energy density was the limiting factor for initiation. Furthermore, as the energy density dropped the energy required for initiation increased markedly. This agrees quite well in a qualitative sense with experimental observations from spark initiated detonations. The experimental program also consisted of two phases. In one of these, reflected initiation of propylene oxide-nitrogen-oxygen mixtures was studied over the temperature range of about 1000-2500°K. The data was correlated to an Arrhenius temperature dependency and yielded an activation energy of approximately 38,000 cal/gm mole. The other experimental study investigated the effect of inhibitors and promotors on the delayed time to ignition for propane-air mixtures, also using the reflected shock technique.

TABLE OF CONTENTS

DIRECT INITIATION OF DETONATION

I INTRODUCTION

The program of research reported here was directed at two Air Force needs, namely the easy evaluation of prospective fuels for fuel-air explosives (FAE) devices as well as the evaluation of fuel tank vulnerability to ignition combustion and detonation from the penetration of hot multi-source gunfire or missile fragments. The common factor for these two needs is that they depend upon the direct initiation of detonation. This phrase means that process during which an igniter causes very rapid transition from the initial quiescent state of a reactive mixture to the final ongoing detonation in the reactive mixture. Hence, if we are to comprehend those events which must occur during the transition process, we shall need to know what exists at the end of the transition process. Thus, we first describe the structure of a self-sustaining propagating detonation wave in considerable detail and then describe our current understanding of initiation behavior. This is followed by sections devoted to details of the work performed under the grant.

II DETONATION STRUCTURE

It is well known that a rather simple, steady-flow hydrodynamic theory (the Chapman-Jouguet or CJ theory) yields a reasonable description of the gross properties of self-sustaining detonation waves.[1] The waves indeed appear to be constant velocity waves traveling at a high supersonic velocity as predicted by the theory and they contain average shock and CJ

plane pressures which are quite adequately predicted by the theory. However, the theory has one rather severe limitation in that it predicts that all exothermic systems should exhibit detonation behavior and, therefore, that there should be no concentration or pressure limits to the propagation of detonation waves. Experimentally, we know that this result is not true. Detonations in tubes do exhibit failure behavior both as the mixture is diluted with inerts and as the initial pressure is reduced. Also, unconfined detonations definitely exhibit concentration limits.

It is now known that the CJ concept only applies to the gross overall behavior. If one looks at the wave structure in sufficient detail, one always finds that the wave is actually propagating with a three-dimensional non-steady structure.[1] This behavior in no way negates the utility of the CJ concept in describing the overall (or gross) behavior of the wave but simply means that we now know that the CJ concept cannot be used to look at detailed structure, just as we already knew that it could not be used to discuss the detailed fluid behavior near the front.

In the past five to ten years we have learned a great deal about the structure of gas phase detonation waves. We now know that a one-dimensional steady wave should not exist because it is hydrodynamically unstable to a perturbation.[2] We also have learned that the instability forms transverse perturbation waves traveling across the front behind the main (or lead) shock wave of the detonation in the flow region which contains the exothermic chemical reactions.[3,4] Further, we know that in an "overall steady" self-sustaining detonation these waves are pressure waves of finite amplitude and propagate with an inherent spacing or structural size which is related to the rate of the chemical reactions that are occurring in the detonation itself.[5]

Since the transverse waves are of finite amplitude, they are actually reasonably weak shock waves (Mach numbers below 1.4) which interact with the lead shock wave to produce Mach stems at their confluence with the front. Furthermore, because of the varying pressure behind the lead shock that is caused by the presence of these waves, the lead shock does not have a constant velocity. The central element of it typically shows a sawtooth-like velocity behavior, with the amplitude varying about ±20 percent of the CJ velocity. This particular behavior occurs while each element of the lead shock wave is decaying at all times with the transverse waves continually overriding these decaying shock elements. When the transverse waves collide, they produce the central shock element whose velocity jumps to a value well above CJ immediately after the intersection of the transverse waves.[6]

The paths of the intersections of the transverse waves with the lead shocks as these shocks propagate produce what is called a detonation cell. A new cell starts with the crossing of oppositely directed transverse waves and the cell ends at the crossing of the next pair of transverse waves in the two trains of these waves.

Generally, the reactions just behind the lead shock are endothermic or thermally neutral before they become exothermic. This distance is called the induction distance and it depends strongly upon the temperature, being shorter the higher the temperature or the higher the shock Mach number. There is an upper limit to the lead shock Mach number, which occurs when M is of the order of 1.5 M_{CJ}, above which the reactions do not become exothermic.

Because the induction distance is finite behind the Mach stem shock created at the start of a new cell, a hot spot is created when the exothermal reactions occur. This hot spot generates a pressure pulse which then

overtakes the Mach stem in the first half of the cell, where it strengthens the shock and thus helps to sustain the detonation. Such a mechanism seems to be a crucial one in order that the detonation can be self-sustaining. There are a number of requirements given here: (1) There must be a collision of transverse waves. (2) The hot spot does not arise until the chemical reactions become exothermic. (3) The resulting pressure pulse must reinforce the lead shock. (4) The reinforcement must occur in the first half of the cell.[7]

Barthel[8] has shown that the cell width or spacing correlates rather well with pressure at various dilutions using an acaustic theory for the origin of the hot spots. The theory requires that caustics associated with two rays collide at the hot spots. The two rays start out in different directions, one going first deeper into the exothermic zone where it turns around, then travels to the shock where it is reflected and subsequently returns to the starting plane; the other first starts toward the shock, reflects, moves past the starting plane and deeper in the exothermic zone to turn around and return to the starting plane. The time to complete this cycle defines a characteristic time τ_a which is intimately related to the characteristic reaction kinetic times.

III INITIATION

As indicated earlier, detonations are usually initiated by means of igniters. Clearly, one of the functions of an igniter is to generate a shock wave of sufficient intensity so that the reactions become fast enough to couple rather closely to the shock. If one can ignore the effects of the

reactions and assume the igniter energy is deposited in an extremely small time, then one can use point source blast wave theory[9] to consider the behavior of the shock. From this theory $R_s \propto t^{2/5}$ and $\dot{R}_s \propto t^{-3/5}$, so the shock starts out at a small radius at an extremely high velocity but subsequently is always decaying. The temperature-time behavior of such a wave is shown in Fig. 1. For early times the temperature is very high and drops rather rapidly as one follows the particle. With reaction, the high temperatures for early times would probably require that the reactions would always be endothermic and the dropping temperature would tend to slow or quench the reactions. When the shock has slowed enough so that the reactions become exothermic at the end of the induction zone, we can introduce the characteristic time, τ_{ind}. For the pressure pulse associated with the end of the induction zone to propagate to the lead shock, we introduce the characteristic time, τ_p. During the time $\tau_{ind} + \tau_p$ the lead shock must not have decayed too much if a cyclic process is to be started. This requirement means then that there must be a minimum value of t_o for the blast wave of Fig. 1, which in turn implies a minimum value of E, the total energy added to create the blast wave.

The studies of Bach, Knystantas and Lee[10] of the direct initiation of detonation using laser pulsed sparks, ordinary electrical sparks, exploding hot wires and exploding high explosive charges as igniters, have shown that the initiation energy required for direct initiation is not constant from technique to technique. Instead, it increases both as the duration of the time for energy deposition increases and as the kernel volume increases. In fact, they found that the important parameter for energy release times which span the 20 nanosecond to 60 microsecond range is not the total energy

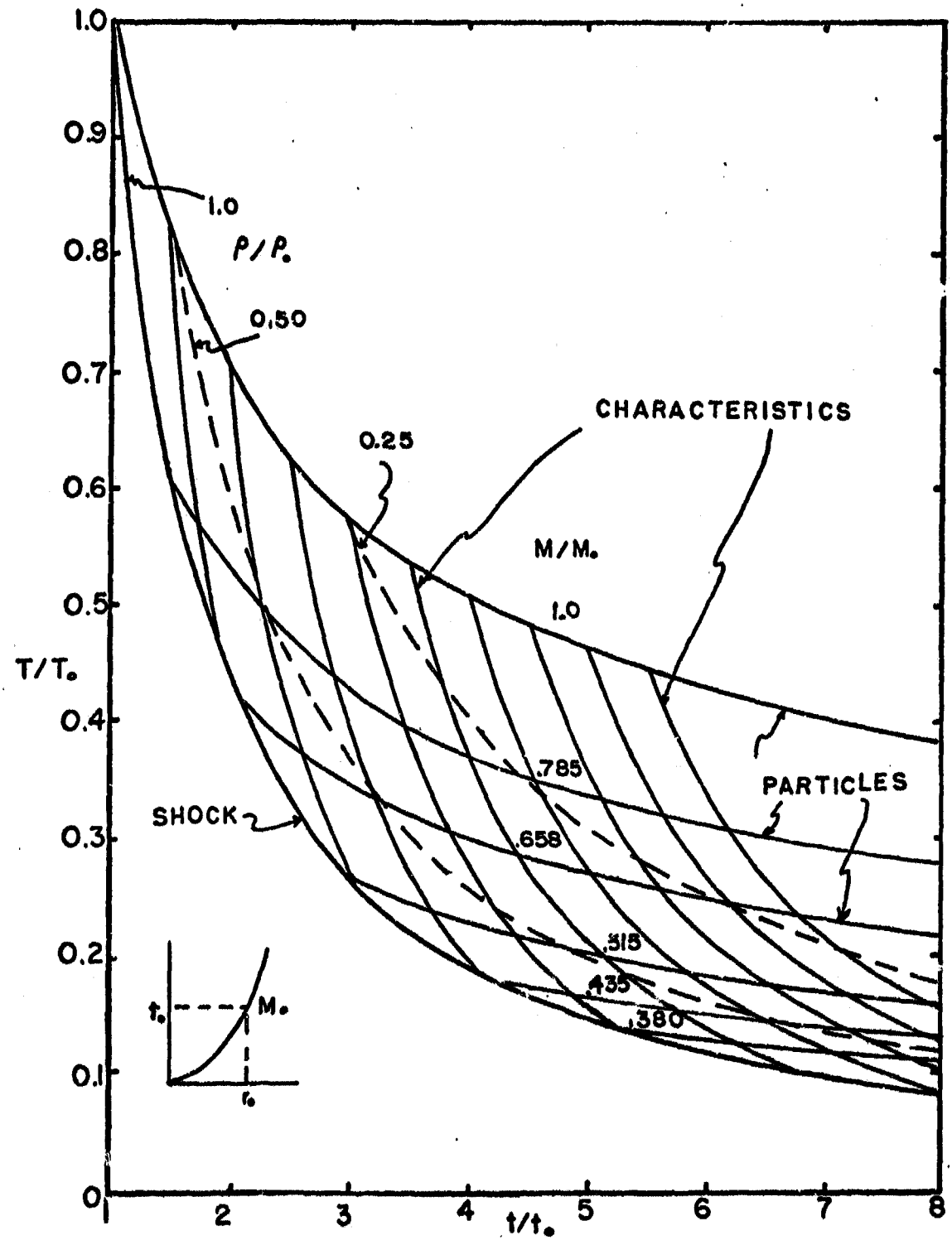

Fig. 1. Temperature along particle path versus time. Characteristics and density are parameters.

deposited but the rate of deposition of energy per unit volume of the kernel, i.e., the power density (energy per unit time per unit volume) of the source. Such a result seems to be more consistent with an expanding piston model in which the piston drives a shock of minimum strength and the power density balances the rate at which energy is expended as work by the piston driving the shock. In this viewpoint, a maximum shock Mach number for the lead shock is reached and this result is much more satisfying than starting off with an infinite Mach number as one must do when one uses ideal point source blast wave theory. This experimental result further suggests that the lead shock wave cannot be modeled as a point source blast wave even though the energy deposition times would seem to indicate that it should be possible to model the shock in this way.

Bach, Knystantas and Lee also found in their studies that if the spherical shock wave is to become a detonation wave, then transverse structure must appear on a lead shock wave that previously had been a smooth spherical wave. If the structure did not appear, the wave decayed until reaction ceased and transition to detonation did not occur. Such a result is quite interesting since the behavior that is observed when initiation is effected is similar to the behavior that is observed during the propagation of actual self-sustaining detonations. It thus strengthens the notion that the transverse structure is essential for the propagation of self-sustaining detonations.

The appearance of structure during the transition to detonation again requires consideration of τ_a if an acoustic origin for the hot spot structure is correct. The value of τ_a will depend upon τ_{ind}, since the latter establishes the distances over which the sound rays must travel. Further, for

a constant Mach number shock, τ_a is greater than τ_p, since the rays for finding the value of the former are inclined to the flow direction as well as making a complete cycle while the ray for finding the value of the latter moves directly along the particle path toward the shock. If the same relationship holds true for a decaying wave, then the parameter $(\tau_{ind} + \tau_a)/t_o$ is a critical parameter for the establishment of structure and for successful transition to detonation.

IV RESEARCH PROGRAM

There are four distinctly different portions of the research program which were conducted under this grant. Two of these are experimental and two are theoretical. The first experimental portion was planned at the start of the grant and consisted of a study to measure the structural size of the transverse wave pattern of self-sustaining detonations in mixtures that were appropriate to the Air Forces'use in FAE devices. This is reported in Section V. The second experimental study was initiated about two years after the start of the grant and consisted of a reflected shock initiation study to determine the effect of promoters and inhibitors on the delay to detonation and rate of heat release in propane-air mixtures and also to determine appropriate delays to detonation and heat release rate for propylene oxide and oxygen-nitrogen mixtures of interest to Dr. John Lee at McGill University. The results of these studies are reported in Section VI.

The first theoretical effort was also anticipated at the start of the grant. In this effort an initiation pulse (a non-ideal blast wave) was to be placed in a reactive system of hydrogen, oxygen and argon. The flow fields

were then to be computed using a full set of reactive equations. On these background fields an acoustic pulse was to be placed and subsequent behavior was then to be followed to see if caustic collisions occurred which depended upon the position and timing of the initial pulse. This material is described in Section VII. After the start of the grant, another theoretical program was initiated. In this program, nonreactive blast wave fields produced by various types of non-ideal sources were used to monitor the initiation behavior using hydrogen-oxygen kinetics. This is reported in Section VIII. Additionally, a number of studies have been made relative to the nature of non-ideal blast waves. The major portion of these studies were supported by a grant from NASA Lewis Laboratories and the Federal Republic of Germany. However, the material has interest to the Air Force needs relative to explosion behaviors and a summary of this work is reported in Section IX.

V THE EFFECT OF MOLECULAR STRUCTURE ON TRANSVERSE WAVE SPACING AND PROPAGATING DETONATION

As an initial part of the program it was decided to study the effect of structure of isomers (same molecular formula, different structure) on the spacing of transverse waves for the isomers of ethylene oxide and propylene oxide. Tables 1, 2 and 3 list the thermochemical properties and structure of these molecules. Ethylene oxide has only one isomer, acetaldehyde, however propylene oxide has five isomers which are listed in Tables 1, 2 and 3. Also in Table 1 the abbreviations that we used for these different species are given.

The results of this study were not very definitive. Figures 2 and 3 represent plots of the cell spacing measured for these various species as a

TABLE 1. Thermochemical Data of Test Isomers

Formula	Name	$\Delta H_{f298°}$ (kcal/mole)	$S°_{298}$ (cal/mole°k)	$\Delta G_{f298°}$ (kcal/mole)	Log k°	Abbreviation
C_2H_4O	Ethylene oxide	-12.58	57.94	- 3.13	2.292	EO
C_2H_4O	Acetaldehyde	-39.76	63.15	-31.86	23.353	ACD
C_3H_6O	Propylene oxide	-22.17	68.53	- 6.16	4.517	PO
C_3H_6O	Trimethylene oxide	-19.25	65.46	- 2.33	1.706	TO
C_3H_6O	Allyl alcohol	-31.55	73.51	-17.03	12.481	AA
C_3H_6O	Acetone	-52.00	70.49	-36.58	26.811	AC
C_3H_6O	Propionaldehyde	-45.90	72.83	-31.18	22.851	PRO
C_3H_6O	Methyl Vinyl Ether	---	---	---	---	MVE

TABLE 2

MOLECULAR STRUCTURES AND PERTINENT DATA OF C_2H_4O ISOMERS: mw. = 44.052

ACETALDEHYDE:

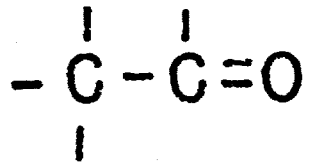

V.P. = 900 torr

B.P. = 20.8 °C

$\Delta H_{f_{298}}$ (g) = −39.76 kcal/mole

ETHYLENE OXIDE:

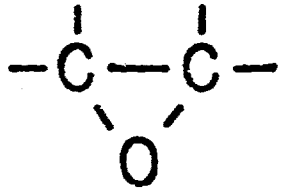

V.P. = 2350 torr

B.P. = 13.5 °C

$\Delta H_{f_{298}}$ (g) = −12.58 kcal/mole

ALL VAPOR PRESSURES (V.P.) ARE AT 25°C

TABLE 3

MOLECULAR STRUCTURES AND PERTINENT DATA OF C_3H_6O ISOMERS: mw = 58.078

PROPYLENE OXIDE:

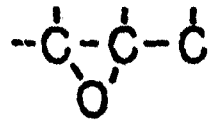

V.P = 555 torr
B.P = 35 °C
ΔH_f (g) = -22.17 kcal/mole

TRIMETHYLENE OXIDE:

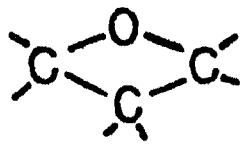

V.P = 325 torr
B.P = 47 °C
ΔH_f (g) = -19.25 kcal/mole

ACETONE:

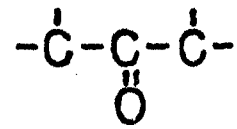

V.P = 229.4 torr
B.P = 56.5 °C
ΔH_f (g) = -52.00 kcal/mole

PROPIONALDEHYDE:

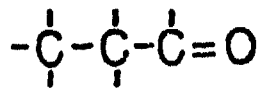

V.P = 285 torr
B.P = 48.8 °C
ΔH_f (g) = -45.90 kcal/mole

ALLYL ALCOHOL:

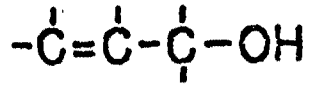

V.P = 28.1 torr
B.P = 97 °C
ΔH_f (g) = -31.55 kcal/mole

METHYL VINYL ETHER:

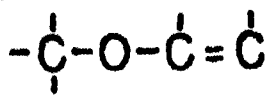

V.P = 2208 torr
B.P = 8.0 °C
ΔH_f (g) = ——

ALL VAPOR PRESSURES (V.P) ARE AT 25 °C
ALL ΔH_f ARE AT 298 °K

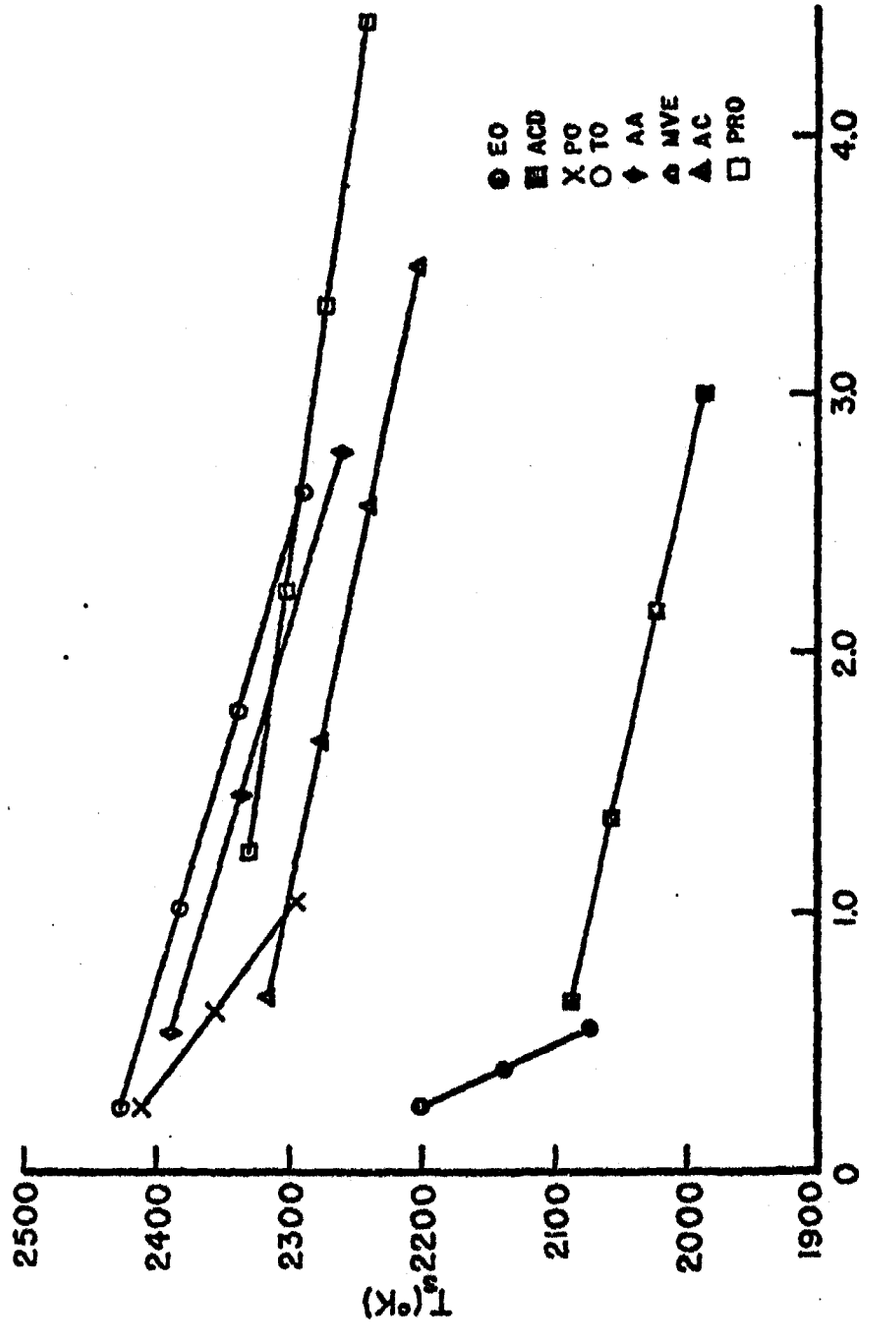

Figure 2. Cell length versus final shock temperature.

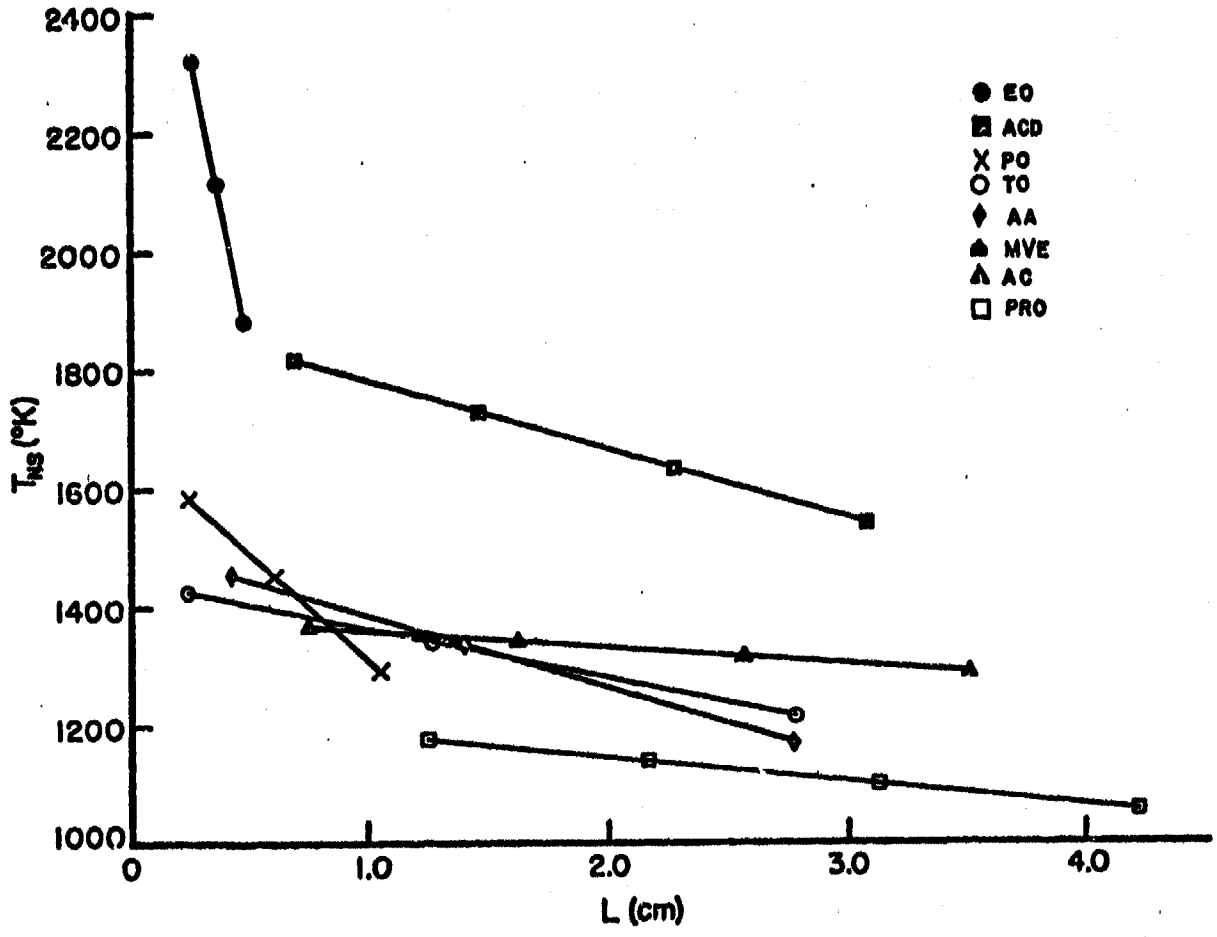

Figure 3. Cell length versus nonreactive shock temperature.

function of both the final shock temperature, i.e., the Chapman-Jouguet temperature of the detonation, and as a function of the initial temperature behind the shock, i.e., the nonreactive shock temperature. Here, the temperature was varied by varying the stoichiometry and dilution in the experiments. The most significant and striking differences are the fact that the slope of the spacing-shock temperature curves is extremely high for both ethylene oxide and propylene oxide and relatively flat for all of the isomers. The conclusion that can be drawn from this study is that both propylene oxide and ethylene oxide are the most reactive isomers in their series. Details of this work are reported in a Master's thesis written by Mr. Delaney.[11]

VI REFLECTED SHOCK INITIATION STUDIES

Two distinct studies were performed in this part of the program. These were initiated by Mr. Joe Foster at Eglin Air Force Base approxiimately two years after the program started. The first of these was a study of the effect of inhibitors or promoters on the ignition delay in a propane-air mixture behind a reflected shock in a conventional shock tube. The second of these was a similar study of initiation behind the reflected shock for a mixture of propylene oxide, oxygen and nitrogen.

The experimental work for both of these studies has been completed. Eventually these two studies will yield two Master's theses describing the results of the studies. These theses are not completed at this time, but should be completed by the Fall of 1977. Copies of these theses will be supplied to the Technical Monitor at the time when they are completed.

VII ACOUSTIC WAVES ON A REACTIVE FLOW

Earlier, we noted that if a decaying spherical shock wave is to become a detonation wave, transverse structure must appear on the initially smooth shock. Also, Barthel[8] had proposed an acoustic mechanism whereby colliding caustics formed hot spots tc initiate the transverse structure in steady planar detonations. Here we examine whether a similar mechanism might be possible for the spherical case.

7.1 Ray Equations

This approach requires that we follow various rays. Hence, following Milne,[12] we write the ray equations as

$$\frac{dx_i}{dt} = an_i + u_i \qquad i = 1, 2, 3 \tag{1}$$

$$\frac{1}{n_i}\left[\frac{dn_i}{dt} + \frac{\partial a}{\partial x_i} + n_k \frac{\partial u_k}{\partial x_i}\right] = \frac{1}{n_j}\left[\frac{dn_j}{dt} + \frac{\partial a}{\partial x_j} + n_k \frac{\partial u_k}{\partial x_j}\right] , \tag{2}$$

where a is the local speed of sound, n_i is the component of the unit normal to the wavefront and u_i is the velocity component. Upon transforming to the spherical case, these become

$$\frac{dr}{dt} = u + a\ell \tag{3}$$

$$\frac{d\psi}{dt} = am/r \tag{4}$$

$$\frac{d\ell}{dt} = -m^2\left[\frac{\partial a}{\partial r} + \ell\frac{\partial u}{\partial r} - (a+\ell u)/r\right] , \tag{5}$$

where ℓ and m are the components in the r and ψ directions of the normal to

the wave front and u is the particle velocity in the radial direction.

Now consider the behavior of $(a+\ell u)/mr$ as a function of time along the ray path. Differentiating the expression as we follow the ray path, we get

$$\frac{d}{dt}\left(\frac{a+\ell u}{mr}\right) = \frac{mr\,\frac{d}{dt}(a+\ell u) - (a+\ell u)\,\frac{d}{dt}(mr)}{m^2r^2}$$

$$= \frac{mr\left\{\frac{\partial a}{\partial t} + \frac{\partial a}{\partial r}\frac{dr}{dt} + \ell\left(\frac{\partial u}{\partial t} + \frac{\partial u}{\partial r}\frac{dr}{dt}\right) + u\frac{d\ell}{dt}\right\} - \left(a + \ell u\right)\left(r\frac{dm}{dt} + m\frac{dr}{dt}\right)}{m^2r^2} \tag{6}$$

Using $\frac{dm}{dt} = -\frac{\ell}{m}\frac{dm}{dt}$ and substituting Eqs. 3, 4 and 5 into Eq. 6, we get

$$\frac{d}{dt}\left(\frac{a+\ell u}{mr}\right) = \frac{1}{mr}\left[\frac{\partial a}{\partial t} + \ell\,\frac{\partial u}{\partial t}\right], \tag{7}$$

Alternatively, the left-hand side of Eq. 7 can be written

$$\frac{d}{dt}\left(\frac{a+\ell u}{mr}\right) = \frac{1}{r}\frac{d}{dt}\left(\frac{a+\ell u}{m}\right) - \frac{a+\ell u}{mr}\frac{dr}{dt}\,. \tag{8}$$

Combining Eqs. 7 and 8, then multiplying by r, we get

$$\frac{d}{dt}\left(\frac{a+\ell u}{m}\right) - \frac{(a+\ell u)}{mr}\frac{dr}{dt} = \frac{1}{m}\left(\frac{\partial a}{\partial t} + \ell\,\frac{\partial u}{\partial t}\right) \tag{9}$$

Hence, if r is large and the right-hand side of Eq. 9 is zero, we obtain the planar equation for steady flow

$$\frac{d}{dt}\left(\frac{a+\ell u}{m}\right) = 0 \tag{10}$$

which has the solution

$$\frac{a+\ell u}{m} = c \tag{11}$$

where c is a constant for each ray.

If the spherical a, u fields are similar to those found in a steady planar detonation, then we can expect colliding caustics. Therefore, for large r, we expect structure in the spherical case.

The behavior for small r is not so apparent, since we have to solve Eq. 7 and it contains unsteady terms. If these unsteady terms are so small that they are negligible compared to r, we obtain

$$\frac{a + \ell u}{mr} = c_1 \tag{12}$$

where c_1 is a constant which is an angular rate. For perhaps some particular a, u fields, we believe this equation could yield colliding caustics. However, whether the unsteady fields created by rapid energy addition in a reactive gas would create such a field can only be determined by numerical integration because of the complexity of the equations.

Our previous success using an implicit integration technique for the steady planar detonation case led us to believe that we might be able to adapt our previous program to the unsteady spherical case with energy addition in the center of the reactive mixture.

7.2 Equations for Reactive Flow

We assumed no diffusion or heat condition occurred in the mixture. Then the species equations for a reactive flow are given by

$$\frac{D[A_i]}{Dt} = \frac{D[A_i]}{Dt}\Big|_R - [A_i]\left[u_r + j\,\frac{u}{r}\right] \qquad , \qquad i=1, \ldots, NSP \tag{13}$$

where $[A_i]$ is the molar concentration of species i, $\frac{D[A_i]}{Dt}\Big|_R$ is the rate of change of concentration due to chemical reaction as we follow a fixed mass

of mixture, j = 0,1,2 for planar, cylindrical and spherical cases, u and u_r are the particle velocity and its spatial derivative and r is the position coordinate. Also $\frac{D}{Dt} = \frac{\partial}{\partial t} + u \frac{\partial}{\partial r}$ is the Euler derivative as we follow the mass.

For our system, the perfect gas law takes the form

$$p = \sum_{i=1}^{NSP} [A_i] RT, \tag{14}$$

where p is the pressure, R is the universal gas constant and T is the absolute temperature.

The molar and mass densities are given by

$$\rho_n = \sum_{i=1}^{NSP} [A_i] \tag{15}$$

$$\rho = \sum_{i=1}^{NSP} MW_i [A_i] \quad , \tag{16}$$

where MW_i is the molecular weight of species i.

From Eqs. 13 and 15, ρ_n obeys the equation

$$\frac{D\rho_n}{Dt} = \sum_{i=1}^{NSP} \frac{D[A_i]}{Dt}\bigg|_R - \rho_n(u_r + j \frac{u}{r}) \tag{17}$$

while from Eqs. 13 and 16, ρ obeys the equation for conservation of overall mass

$$\frac{D\rho}{Dt} = - \rho(u_r + j \frac{u}{r}) \quad . \tag{18}$$

The first law is written as

$$\frac{Dh}{Dt} - \frac{1}{\rho}\frac{Dp}{Dt} = \dot{q} \quad , \tag{19}$$

where $h = \sum_{i=1}^{NSP} [A_i]h_i/\rho$ is the enthalpy per unit mass of mixture, h_i is the enthalpy per mole of species i, and $\dot{q}$ is the rate of energy per unit mass added from outside the system. We further assume that h_i is a function of T only, with $h_i = h_i(T)$ and $\frac{\partial h_i}{\partial T} = c_{p_i}(T)$.

From Eq. 19 and the relationship for h, we obtain

$$\frac{DT}{Dt} = \frac{\sum_{i=1}^{NSP} \left[T - \frac{h_i}{R}\right] \left.\frac{D[A_i]}{Dt}\right|_R - \rho_n T(u_r + j\frac{u}{r}) + \rho\dot{q}/R}{\sum_{i=1}^{NSP} [A_i][c_{p_i}/R - 1]} \quad . \tag{20}$$

The momentum equation is given by

$$\frac{Du}{Dt} = -\frac{p_r}{\rho} \quad . \tag{21}$$

The particle path is given by

$$\frac{Dr}{Dt} = u \quad . \tag{22}$$

The right-hand side of the equations for $[A_i]$, T, u and r contain the variables $[A_i]$, T, u, r, u_r and p_r if $\dot{q}$ is specified as a function of these variables as well as of time. For explicit programs, u_r and p_r need only be calculated at time $t = t_n$ to find the variables at $t = t_{n+1}$, for we have NSP + 3 equations to calculate NSP + 3 dependent variables. However, the set

of equations is mathematically a set of "stiff" differential equations which often exhibit numerical stability problems during their integration unless very small step sizes are taken. In an effort to avoid this difficulty, we turned to an implicit method.

7.3 Implicit Methods

The concept of the implicit method[13] is basically as follows. We have a set of differential equations

$$\frac{dy_i}{dt} = f_i(y_j,t) \qquad i,j = 1, \ldots, N \ . \tag{23}$$

We know the values y_j at time $t = t_n$. We wish their values at time $t = t_{n+1}$. Let us define $h_{n+1} = t_{n+1} - t_n$ and $K_{i,n+1} = y_{i,n+1} - y_{i,n}$. Then, we assume an implicit expansion, such as

$$K_{i,n+1} = \frac{1}{2}\left(\frac{dy_{i,n+1}}{dt} + \frac{dy_{i,n}}{dt}\right) h_{n+1} = \frac{dy_{i,n+1}}{dt} + \frac{1}{2}\left\{\frac{dy_{i,n+1}}{dt} - \frac{dy_{i,n}}{dt}\right\} h_{n+1} \tag{24}$$

Eq. 24 is implicit because $\frac{dy_{i,n+1}}{dt}$ depends upon the values of y_j at time t_{n+1}, so are not known yet. But

$$\frac{dy_{i,n+1}}{dt} - \frac{dy_{i,n}}{dt} = \frac{d^2y_{i,n}}{dt^2} h_{n+1} + \ldots .$$

$$= \left[\frac{\partial}{\partial t}\frac{dy_{i,n}}{dt} + \sum_{j=1}^{N} \frac{\partial}{\partial y_j}\left(\frac{dy_{j,n}}{dt}\right)\frac{dy_{j,n}}{dt}\right] h_{n+1} \tag{25}$$

Let $\frac{\partial}{\partial t}\frac{dy_{i,n}}{dt} = g_{i,n}$ and $\frac{\partial}{\partial y_j}\frac{dy_{i,n}}{dt} = \beta_{i,j}$. Then Eq. 25 becomes

$$\frac{dy_{i,n+1}}{dt} - \frac{dy_{i,n}}{dt} = g_{i,n}h_{n+1} + \sum_{j=1}^{N} \beta_{i,j} \frac{dy_{j,n}}{dt} h_{n+1} \quad . \tag{26}$$

If we use Eq. 24, Eq. 26 becomes

$$\begin{aligned}
\frac{dy_{i,n+1}}{dt} - \frac{dy_{i,n}}{dt} &= g_{i,n}h_{n+1} + \sum_{j=1}^{N} \beta_{i,j} \left\{ K_{j,n} - \frac{h_{n+1}}{2} \left[\frac{dy_{j,n+1}}{dt} - \frac{dy_{j,n}}{dt} \right] \right\} \\
&= g_{i,n}h_{n+1} + \sum_{j=1}^{N} \beta_{i,j} \left\{ K_{j,n} - \frac{h_{n+1}}{2} \left[g_{j,n}h_{n+1} \right.\right. \\
&\qquad \left.\left. + \beta_{j,k} \left(K_{k,n} - \frac{h_{n+1}}{2} \left[\frac{dy_{k,n+1}}{dt} - \frac{dy_{k,n}}{dt} \right] \right) \right] \right\} \\
&= g_{i,n}h_{n+1} - \sum_{j=1}^{N} \beta_{i,j} g_{j,n} \frac{h_{n+1}^2}{2} + \sum_{j=1}^{N} \left(\beta_{i,j} - \frac{h_{n+1}}{2} \alpha_{i,j} \right) K_{j,n}
\end{aligned} \tag{27}$$

where $\alpha_{i,j} = \sum_{k=1}^{N} \beta_{i,k}\beta_{k,j}$. Putting Eq. 27 back into Eq. 24, we get

$$K_{i,n+1} - \frac{h_{n+1}}{2} \sum_{j=1}^{N} \left(\beta_{i,j} - \frac{h_{n+1}}{2} \alpha_{i,j} \right) K_{j,n} = f_{i,n}h_{n+1} + \frac{h_{n+1}^2}{2} \left[g_{i,n} - \frac{h_{n+1}}{2} \sum_{j=1}^{N} \beta_{i,j} g_{j,n} \right] \tag{28}$$

which is a coupled set of N linear algebraic equations in $K_{j,n+1}$. Upon solving for $K_{i,n+1}$, then $y_{i,n+1}$ is easily obtained from

$$y_{i,n+1} = y_{i,n} + K_{i,n+1} \quad . \tag{29}$$

7.4 Closure Considerations

From the preceding theory, it appears that equations for $\frac{Du_r}{Dt}$ and $\frac{Dp_r}{Dt}$ are needed. We attempt now to derive them by using the relationship

$$\frac{D\psi_r}{Dt} = \frac{\partial}{\partial r}\frac{D\psi}{Dt} - u_r\psi_r \quad . \tag{30}$$

Applying this equation with $\psi = u$, we get

$$\frac{Du_r}{Dt} = \frac{\partial}{\partial r}\left(-\frac{p_r}{\rho}\right) - u_r^2 = -\frac{p_{rr}}{\rho} + \frac{p_r\rho_r}{\rho^2} - u_r^2 \quad . \tag{31}$$

Thus we now have two additional variables p_{rr} and ρ_r. Clearly, to follow such a scheme will not lead to closure.

Rather, closure is to be accomplished by a different scheme. We integrate along a path from the point i-1,n to the point i,n+1 or from point i+1,n to the point i,n+1 by using

$$\frac{\delta K_r^+}{\delta t} = u + K^+a \tag{32}$$

and

$$\frac{\delta K_r^-}{\delta t} = u - K^-a \quad , \tag{33}$$

which is much like integrating along characteristics except it is more convenient to move from computed points on the $t = t_n$ time line to avoid interpolation between points on this time line as required when integrating along characteristics. Further, because we now have two new variables K^+ and K^-, we also integrate the equations

$$\frac{\delta K_u^+}{\delta t} = \frac{Du}{Dt} + K^+au_r = -\frac{p_r}{\rho} + K^+au_r \quad , \tag{34}$$

$$\frac{\delta K_u^-}{\delta t} = \frac{Du}{Dt} - K^- a u_r = -\frac{p_r}{\rho} - K^- a u_r \quad , \tag{35}$$

$$\frac{\delta K_p^+}{\delta t} = \frac{Dp}{Dt} + K^+ a p_r \quad , \tag{36}$$

$$\frac{\delta K_p^-}{\delta t} = \frac{DP}{Dt} - K^- a p_r \quad , \tag{37}$$

$$\frac{Dp}{Dt} = \frac{R\left\{T \sum_{i=1}^{NSP} \frac{D[A_i]}{Dt}\bigg|_R \times \sum_{i=1}^{NSP} [A_i] \frac{c_{p_i}}{R} - \rho_n \sum h_i \frac{D[A_i]}{Dt}\bigg|_R + \rho\rho n\dot{q}/R\right\} - \rho a^2 (u_r + \frac{ju}{r})}{\sum_{i=1}^{NSP} [A_i]\left[\frac{c_{p_i}}{R} - 1\right]} \tag{38}$$

and a in Eqs. 32-38 is the frozen speed of sound given by

$$a^2 = \frac{\sum_{i=1}^{NSP} [A_i] \frac{c_{p_i}}{R}}{\sum_{i=1}^{N} [A_i]\left[\frac{c_{p_i}}{R} - 1\right]} \frac{\rho_n}{\rho} RT \tag{39}$$

Now it appears that the system is overspecified, but the extra equations are used for checking purposes. However, we also will note here that care must be exercised in the integration of Eqs. 32-38 but the discussion of this problem will be deferred to a later section. We see though, that upon integration, one can find expressions for K^-, K^+, $u_r(i,n+1)$ and $p_r(i,n+1)$ in terms of $[A_i]$, u, r and T at the new time, so sufficient equations are at hand.

7.5 Mixture and Reactions

For all calculations, the system was assumed to be 70% argon and 30% of a stoichiometric mixture of hydrogen and oxygen. For this system, the

reactions and rate constants given in Table 4 were used.[14]

7.6 Initial Conditions and Boundary Conditions

The initial conditions were that the mixture was at rest, with uniform composition, pressure and temperature throughout. The initial pressure was 200 Torr and the initial temperature was 300°K.

The boundary conditions were specified at r = 0 and at the moving wave forming the outer boundary.

At r = 0, symmetry requires $u = p_r = [A_i]_r = T_r = 0$.

The outer boundary may be either an acoustic wave or a shock wave. If the former, its path is given by

$$r_f = r_c(0) + a_o t \quad , \tag{40}$$

where r_f is the position of the front at time t and $r_c(0)$ is the origin of the wave. Because of the nonlinear nature of the flow, the acoustic wave will gradually get steeper and ultimately become a shock. To determine when this transition occurs, we assume no reaction and note that before transition, $p_f = p_o$ and $u_f = 0$ for all points along the front. Whence

$$\left.\frac{\delta^+ u}{\delta t}\right|_f = \left.\frac{Du}{Dt}\right|_f + a u_r\Big|_f = -\frac{p_{r_f}}{\rho_o} + a_o u_{r_f} = 0 \quad , \tag{41}$$

so
$$p_{r_f} = \rho_o a_o u_{r_f} \tag{42}$$

on the front. Since Eq. 42 holds for every point on the front, then

$$\left.\frac{\delta^+ p_r}{\delta t}\right|_f = \rho_o a_o \frac{\delta^+ u_r}{\delta t} \tag{43}$$

TABLE 4. The reaction equations and rate constants used in the Rayleigh program. The rate equations are of the form $K_i = Z_i T^n \exp(E_i/RT)$.

Reactants	Products	Z_i [a]	n	E_i [b]
$O_2 + M$	$O + O + M$	3.56 D 15	0	1.18 D 05
$O + O + M$	$O_2 + M$	2.00 D 14	0	0.0
$H_2 + M$	$H + H + M$	3.10 D 15	0	1.10 D 05
$H + H + M$	$H_2 + M$	6.50 D 14	0	0.0
$O_2 + H$	$O + OH$	2.24 D 14	0	1.68 D 04
$OH + O$	$O_2 + H$	1.30 D 13	0	0.0
$HO_2 + M$	$O_2 + H + M$	2.40 D 15	0	4.59 D 04
$O_2 + H + M$	$HO_2 + M$	1.59 D 15	0	-1.00 D 03
$H_2 + O$	$OH + H$	1.74 D 13	0	9.45 D 03
$H + OH$	$H_2 + O$	7.33 D 12	0	7.30 D 03
$H_2O + H$	$H_2 + OH$	8.41 D 13	0	2.01 D 04
$H_2 + OH$	$H_2O + H$	2.19 D 13	0	5.15 D 03
$H_2O + O$	$OH + OH$	5.75 D 13	0	1.80 D 04
$OH + OH$	$H_2O + O$	5.75 D 12	0	7.80 D 02
$H_2O + M$	$H + OH + M$	1.00 D 17	0	1.17 D 05
$OH + H + H_2O$	$H_2O + H_2O$	1.17 D 17	0	0.0
$OH + H + H_2$	$H_2O + H_2$	2.92 D 16	0	0.0
$OH + H + O_2$	$H_2O + O_2$	2.92 D 16	0	0.0
$OH + H + AR$	$H_2O + AR$	7.02 D 15	0	0.0
$H_2O_2 + H$	$H_2 + HO_2$	2.34 D 13	0	9.20 D 03
$H_2 + HO_2$	$H_2O_2 + H$	9.60 D 12	0	2.40 D 04
$H_2O_2 + OH$	$H_2O + HO_2$	1.00 D 13	0	1.80 D 03
$H_2O + HO_2$	$H_2O_2 + OH$	2.80 D 13	0	3.27 D 04
$H_2O_2 + M$	$OH + OH + M$	1.20 D 17	0	4.55 D 04
$OH + OH + M$	$H_2O_2 + M$	8.40 D 14	0	-5.30 D 03
$H_2O_2 + H$	$H_2O + OH$	3.18 D 14	0	9.00 D 03
$H_2O + OH$	$H_2O_2 + H$	5.60 D 13	0	7.79 D 04

[a] (cm^3/mole/sec or cm^6/$mole^2$/sec).

[b] (cal/mole).

along the front. Consequently,

$$\left.\frac{\delta^+ p_r}{\delta t}\right|_f = \frac{\partial}{\partial r}\left(\frac{Dp}{Dt}\right)_f - u_r p_r\Big|_f^+ + a p_{rr}\Big|_f = -\gamma p_r\left(u_r + j\frac{u}{r}\right)_f - \gamma p_o\left[u_{rr} + j\left(\frac{u_r}{r} - \frac{u}{r}\right)\right]_f$$

$$- \gamma p_r\left(u_r - j\frac{u}{r}\right)_f - u_r\left(\rho_o a_o u_r\right)_f + a_o p_{rr_f} = \rho_o a_o\left[\frac{\partial}{\partial r}\frac{Du}{Dt} - u_r^2 + a u_{rr}\right]_f$$

$$= \rho_o a_o\left[-\frac{p_{rr_f}}{\rho_o} + \frac{p_{r_f}\rho_{r_f}}{\rho_o^2} - u_{r_f}^2 + a_o u_{rr_f}\right] . \qquad (44)$$

We have also made the assumption that $\dot{q} = 0$ at the front, so the flow is isentropic in that region and therefore $\frac{p_r}{p} = \frac{\gamma\rho_r}{\rho}$. Consequently $\rho_{r_f} = \frac{p_{r_f}}{a_o^2} = \frac{\rho_o u_{r_f}}{a_o}$ leads to the following relationship between p_{rr_f} and u_{rr_f} from Eq. 44.

$$p_{rr_f} = \rho_o a_o\left[u_{rr_f} + \frac{u_{r_f}}{a_o} + \frac{j}{2}\frac{u_{r_f}}{r_f}\right] . \qquad (45)$$

Putting this result into the equation for $\frac{\delta^+ u_r}{\delta t}$, we have

$$\left.\frac{\delta^+ u_r}{\delta t}\right|_f = -\left[\left(\frac{\gamma+1}{2}\right)u_{r_f}^2 + \frac{j}{2}a_o\frac{u_{r_f}}{r_f}\right] , \qquad (46)$$

which can be written as

$$\frac{\delta^+\left(\frac{1}{u_{r_f}}\right)}{\delta t} - \frac{j}{2}\frac{a_o}{r_f}\left(\frac{1}{u_{r_f}}\right) = \frac{\gamma+1}{2} . \qquad (47)$$

Eq. 47 has the integrating factor $\exp\left[-\frac{j}{2}\int\frac{a_o}{r_f}\,dt\right] = [r_c(o) + a_o t]^{-j/2}$ so the solution of Eq. 46 is

$$\frac{1}{u_r[r_c(o)+a_o t]^{j/2}} = C_i + \frac{\gamma+1}{2}\int\frac{dt}{[r_o+a_o t]^{j/2}} \quad . \tag{48}$$

For the spherical case with $j = 2$, the last integral becomes $\frac{\gamma+1}{2a_o}\ln[r_c(o)+a_o t]$. If at $t = t_1$, $u_{r_f} = u_{r_1}$,

$$u_{r_f} = \frac{\frac{2}{\gamma+1}}{\left[r_c(o)+a_o t\right]\left[\frac{-\frac{2}{\gamma+1}}{u_{r_1}(r_c(o)+a_o t_1)} + \frac{1}{a_o}\ln\left(\frac{r_c(o)+a_o t}{r_c(o)+a_o t_1}\right)\right]} \quad . \tag{49}$$

If $r_c = 0$, this becomes

$$u_{r_f} = \frac{\frac{2}{\gamma+1}}{t\left[\frac{\frac{2}{\gamma+1}}{u_{r_1} t_1} + \ln\frac{t}{t_1}\right]} \quad . \tag{50}$$

But the shock wave forms as $u_{r_f} \to \infty$, or from Eq. 50,

$$\frac{t}{t_1} = \exp - \left(\frac{\frac{2}{\gamma+1}}{u_{r_1} t_1}\right) \quad , \tag{51}$$

and since $u_{r_1} < 0$, a shock forms in a finite time larger than t_1.

Alternatively, it may happen that before this value of t is reached, an interior shock overtakes the leading acoustic front. In that case, thereafter the shock equations must be satisfied at the outer boundary, with constant pressure, density and temperature and zero velocity ahead of the shock. Since these conditions pertain to a special case of a shock wave moving into

a reacting fluid, the theory for this general case is considered next.

7.7 Shock Wave in a Reacting Fluid

In a system moving with the shock, the conservation equations may be written

$$\rho_a w_s = \rho_b [w_s \pm (u_a - u_b)] \tag{52}$$

$$p_a + \rho_a w_s^2 - p_b + \rho_b [w_s \pm (u_a - u_b)]^2 \tag{53}$$

$$h_a + w_s^2/2 = h_b + [w_s \pm (u_a - u_b)]^2/2 \quad , \tag{54}$$

where the subscripts a and b refer to conditions ahead of and behind the shock, w_s is the velocity of the shock relative to the fluid ahead and the plus-minus signs refer to outwardly and inwardly moving shocks. We also have

$$h = \sum_{i=1}^{NSP} [A_i] h_i / \rho \tag{55}$$

$$\rho = \sum_{i=1}^{NSP} [A_i] MW_i \tag{56}$$

$$\rho_n = \sum_{i=1}^{NSP} [A_i] \tag{57}$$

$$p = \rho_n RT \tag{58}$$

$$a_f^2 = \gamma \frac{\rho_n}{\rho} RT \tag{59}$$

$$c_p = \frac{\sum_{i=1}^{NSP} [A_i] c_{p_i}}{\rho} \tag{60}$$

$$c_v = \frac{\Sigma [A_i] c_{v_i}}{\rho} \tag{61}$$

$$c_p - c_v = R \tag{62}$$

$$\gamma = c_p / c_v \tag{63}$$

We further make the assumption that the flow is frozen while crossing the shock, so

$$\frac{[A_i]_b MW_i}{\rho_b} = \frac{[A_i]_a MW_i}{\rho_a} \tag{64}$$

Hence

$$\frac{[A_i]_b}{\rho_b} = \frac{[A_i]_a}{\rho_a} \tag{65}$$

and

$$\frac{\rho_{n_b}}{\rho_b} = \frac{\rho_{n_a}}{\rho_a} \quad , \tag{66}$$

which means that the molecular weight does not change on crossing the shock. There are now sufficient equations for solving for the flow conditions behind the shock in terms of w_s and flow conditions ahead.

In order to find the spatial derivatives u_r and p_r behind the shock, we differentiate Eqs. 52, 53, 54, 55, 58, 65 and 66 while following the shock to get

$$\frac{\delta^s \rho_a}{\delta t} w_s + \rho_a \frac{\delta^s w_s}{\delta t} = \frac{\delta^s \rho_b}{\delta t} [w_s \pm (w_a - u_b)] + \rho_b \left[\frac{\delta^s w_s}{\delta t} \pm \left(\frac{\delta^s u_a}{\delta t} - \frac{\delta^s u_b}{\delta t} \right) \right] , \tag{67}$$

$$\frac{\delta^s p_a}{\delta t} + \frac{\delta^s \rho_a}{\delta t} w_s^2 + 2\rho_a w_s \frac{\delta^s w_s}{\delta t} = \frac{\delta^s p_b}{\delta t} + \frac{\delta^s \rho_b}{\delta t} [w_s \pm (u_a - u_b)]^2$$

$$+ 2 \rho_b [w_s \pm (u_a - u_b)] \left[\frac{\delta^s w_s}{\delta t} \pm \left(\frac{\delta^s u_a}{\delta t} - \frac{\delta^s u_b}{\delta t} \right) \right] ,$$

(68)

$$\frac{\delta^s h_a}{\delta t} + w_s \frac{\delta^s w_s}{\delta t} = \frac{\delta^s h_b}{\delta t} + [w_s \pm (u_a - u_b)] \left[\frac{\delta^s w_s}{\delta t} \pm \left(\frac{\delta^s u_a}{\delta t} - \frac{\delta^s u_b}{\delta t} \right) \right] , \tag{69}$$

$$\frac{\delta^s h_b}{t} = \frac{\Sigma [A_i] c_{p_i}}{\rho} \frac{\delta^s T_b}{\delta t} - \frac{h_b}{\rho_b} \frac{\delta^s \rho_b}{\delta t} + \sum \frac{h_{i_b}}{\rho_b} \frac{\delta^s [A_i]_b}{\delta t} , \tag{70}$$

$$\frac{\delta^s p_b}{\delta t} = R \left[\rho_{n_b} \frac{\delta^s T_b}{\delta t} + T_b \frac{\delta^s \rho_{n_b}}{\delta t} \right] , \tag{71}$$

$$\frac{1}{\rho_b} \frac{\delta^s [A_i]_b}{\delta t} - \frac{[A_i]_b}{\rho_b^2} \frac{\delta^s \rho_b}{\delta t} = \frac{1}{\rho_a} \frac{\delta^s [A_i]_a}{\delta t} - \frac{[A_i]_a}{\rho_a^2} \frac{\delta^s \rho_a}{\delta t} , \tag{72}$$

$$\frac{1}{\rho_b} \frac{\delta \rho n_b}{\delta t} - \frac{\rho n_b}{\rho_b^2} \frac{\delta^s \rho_b}{\delta t} = \frac{1}{\rho_a} \frac{\delta^s \rho_{n_a}}{\delta t} - \frac{\rho_{n_a}}{\rho^2} \frac{\delta^s \rho_a}{\delta t} , \tag{73}$$

where the derivatives ahead of the shock have the form

$$\frac{\delta^s \psi_a}{\delta t} = \frac{D\psi_a}{Dt} + (\dot{r}_s - u_a) \frac{\partial \psi_a}{\partial r} = \frac{D\psi_a}{Dt} \pm w_s \frac{\partial \psi_a}{\partial r} , \tag{74}$$

derivatives behind the shock have the form

$$\frac{\delta^s \psi_b}{\delta t} = \frac{D\psi_b}{Dt} + (\dot{r}_s - u_b)\frac{\partial \psi_b}{\partial r} = \frac{D\psi_b}{Dt} \pm [w_s \pm (u_a - u_b)]\frac{\partial \psi_b}{\partial r} \qquad (75)$$

and the derivative $\frac{\delta^s w_s}{\delta t}$ is given by

$$\frac{\delta^s w_s}{\delta t} = \mp \left(\ddot{r}_s - \frac{\delta^s u_a}{\delta t}\right) \quad , \qquad (76)$$

with r_s being the shock position coordinate.

The set of (NSP+6) equations, 67-73, is now solved for $\frac{\delta^s p_b}{\delta t}$ and $\frac{\delta^s u_b}{\delta t}$ in terms of $\frac{\delta^s w_s}{\delta t}$ and derivatives ahead of the shock. When $\frac{\delta^s p_b}{\delta t}$ and $\frac{\delta^s u_b}{\delta t}$ are written in the form of Eq. 75, they contain only the two unknowns u_{r_b} and p_{r_b}, so simultaneous solution of these two equations will yield values for u_{r_b} and p_{r_b}.

7.8 Specification of $\dot{q}$

The rate of energy input was assumed to have the form

$$\dot{q} = \dot{q}_o \, X\,(r, r_c(t))\phi(t) \quad , \qquad (77)$$

where $\dot{q}_o$ is a constant and $r_c(t)$ is the outer edge of the core in which energy is being added. For all work undertaken in these studies, ϕ had the form

$$(t) = \exp(-t/\tau_1) - \exp(t/\tau_2) \quad , \qquad (78)$$

where τ_1 and τ_2 are decay parameters or shaping constants. In addition, $r_c(t)$ had the form

$$r_c(t) = f_o t^{\alpha} \quad , \tag{79}$$

with f_o being a constant and the exponent α was within the range $0 < \alpha < 1$.

Initially, $X(r,r_c)$ was chosen to be the function

$$\begin{aligned} X &= r_c^3 - r^3 \ . && 0 \le r \le r_c \\ &= 0 && r_c < r < \infty \end{aligned} \tag{80}$$

This choice for X turned out to be an unfortunate one, for at $r = r_c$ there is a jump in $\dot{q}_r$. This discontinuity led to difficulty in the computing program. The specific difficulty and the theory will be given in later sections.

7.9 Additional Computational Matters

Since an implicit method for integration of a set of differential equations is usually slower and more costly than an explicit method, to keep costs down the maximum number of particles to be followed was limited to 60. When the number of particles followed approached 60, the flow field was rezoned to a smaller number before calculation at the next time line started.

Four types of points occurred in the calculation, namely, (1) origin, (2) interior, (3) shock and (4) outer boundary. The treatment at the origin had to be special because the boundary conditions require that the particle motion and momentum equations be dropped from the set to be integrated. Shock points and outer boundary points also had to be treated as special cases.

With the above scheme and the assumed X function, difficulty in starting the computation was experienced. Considerable effort was devoted to trying to use similarity variables to overcome the starting problem, but this effort was unsuccessful. Finally, because of doubts about whether the

implicit method could be used for starting the computation, we turned to the CLOUD program of A. K. Oppenheim as modified by A. A. Adamczyk.[15] After a few time lines were calculated using this program, negative velocities began to appear near the origin and unstable oscillations appeared in the flow. These oscillations usually became so large that the program would fail. The origin of this behavior was traced to the particular X function assumed. When a new X function was chosen, given by

$$X = r_c^3 - 3r_c r^2 + 2r^3 \quad , \tag{81}$$

these troubles disappeared. It should be noted in this case that $\dot{q}_r$ is zero at $r = r_c$.

A second difficulty encountered in using the CLOUD program was that u_r and p_r derived from curve-fitting the values of u and p as a function of radius did not vary smoothly with radius. The difficulty was traced to roundoff error and overcome by recasting the calculations for the dimensionless pressure, specific energy and specific volume, $\bar{p}$, $\bar{e}$ and $\bar{v}$ respectively, in terms of the reduced variables $\bar{p}$-1, $\bar{e}-\bar{e}_o$ and $\bar{v}$-1, where $\bar{e}_o$ was the initial dimensionless specific energy, $\frac{1}{\gamma-1}$.

One of these time lines was chosen to be the starting line for the implicit program. The particular time line chosen was one in which the temperature in the core had been raised less than 0.5°K, so no significant reaction could have yet taken place.

7.10 Effects of Discontinuities in $\dot{q}$ and $\dot{q}_r$

This section summarizes results submitted elsewhere.[16] Basically, we sought to explore what effect discontinuities in $\dot{q}$ or $\dot{q}_r$ occurring along

$\dot{r}_c = u+ka$ would have on the solutions of the set of equations

$$\frac{Dv}{Dt} = v(u_r + j\frac{u}{r}) \quad , \tag{82}$$

$$\frac{Du}{Dt} = -vp_r \quad , \tag{83}$$

$$\frac{De}{Dt} = -(\gamma-1)e(u_r + j\frac{u}{r}) + \dot{q} \quad , \tag{84}$$

$$\frac{Dp}{Dt} = -\gamma p(u_r + j\frac{u}{r}) + (\gamma-1)\dot{q}/v \quad , \tag{85}$$

and

$$pv = (\gamma-1)e \tag{86}$$

near the discontinuity.

The representation of these discontinuities in $\dot{q}$ or $\dot{q}_r$ are shown in Fig. 4. The particular effects on p, u, e and c are dependent upon the value of k. If $k = 0$, then we have a behavior like a contact discontinuity. If $k \neq 0$, then the effect is wavelike.

A jump in a variable will be indicated by the usual convention of brackets, such as

$$[u] = u_2 - u_1$$

where the subscripts 2 and 1 refer to points just inside and outside the $r = r_c$ surface.

The derivative following a variable, ψ, along the interface is given by

$$\frac{\delta\psi}{\delta t} = \frac{\partial\psi}{\partial t} + r_e\frac{\partial\psi}{\partial r} = \frac{D\psi}{Dt} + (\dot{r}_e - u)\frac{\partial\psi}{\partial r} \quad . \tag{87}$$

Also, we repeat the equation

$$\frac{D\psi_r}{Dt} = \frac{\partial}{\partial r}\frac{D\psi}{Dt} - u_r\psi_r \quad . \tag{88}$$

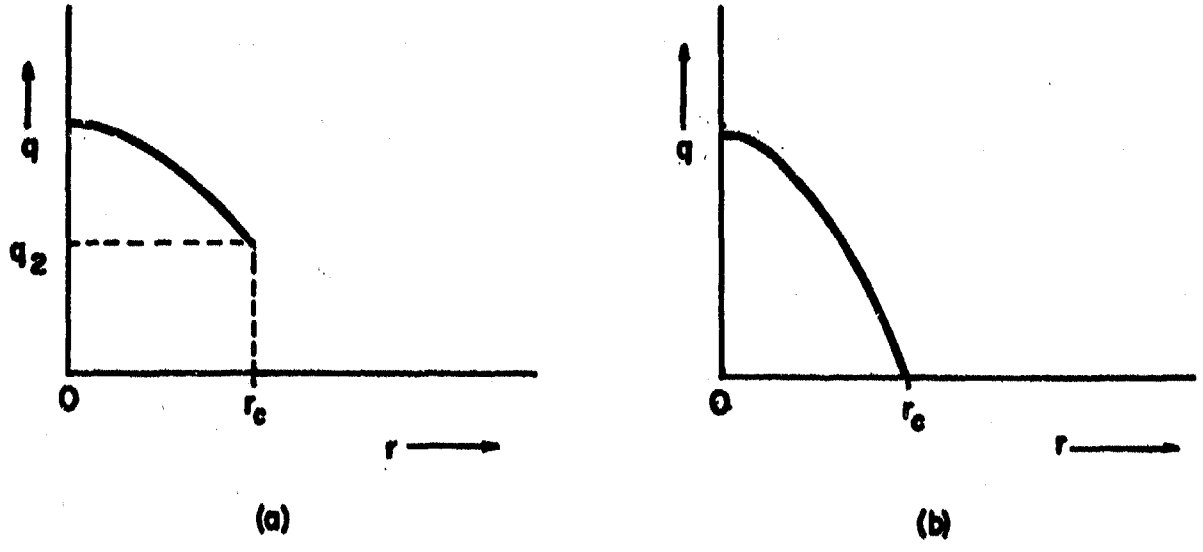

Fig. 4. The assumed behavior of the energy addition rate q vs radial distance r. For (a) q and q_r are both discontinuous at the kernel edge while for (b) q is continuous but q_r is discontinuous at the edge.

a) Contact Surface

In this case, $k = 0$, so $\dot{r}_c = u$ and pressure and velocity must be continuous across the interface. For a jump in $\dot{q}$, we form

$$\frac{\partial[p]}{\partial t} = -\gamma p_2[u_r] + (\gamma-1)\dot{q}_2 v_2 = 0 \quad , \tag{89}$$

so

$$[u_r] = (\gamma-1)\dot{q}_2/\gamma p_2 r_2 = \dot{q}_2/\gamma e_2 \quad , \tag{90}$$

Using this result, we can find that the equation for [e] is

$$\frac{\delta[e]}{\delta t} = -(\gamma-1)[e](ur_1 + ju_1/r_c) + \dot{q}_2/\gamma \quad , \tag{91}$$

which formally has the solution

$$[e] = \exp\{-A(t)\}\{c_1 + \frac{1}{\gamma}\int_0^t \dot{q}_2 \exp\{A(\tau)\}d\tau\}, \tag{92}$$

where

$$A(t) = (\gamma-1)\int_0^t (u_{r_1} + u_1/r_c)d\tau \quad . \tag{93}$$

With quiescent initial flow, c_1 is zero and we find that [e] is positive, which intuitively is the expected behavior.

From Eq. 86 we get

$$[v] = v_1/e_1[e] \quad , \tag{94}$$

so [v] is also positive.

Turning now to Eq. 83, we write

$$\frac{\delta[u]}{\delta t} = -(v_2 p_{r_2} - v_1 p_{r_1}) = 0 \quad . \tag{95}$$

Hence, there is no jump in vp_r but there is a jump in p_r given by

$$[p_r] = \left(\frac{v_i}{v_2}-1\right) p_{r_1} = - p_{r_1}[e]/e_2 \quad , \tag{96}$$

which is positive, since p_{r_1} is negative and [e] is positive.

The results are depicted in Fig. 5.

For $\dot{q} = 0$ but a jump in $\dot{q}_r$ at r_c, we have no jumps in u_r, e, v and p_r. We now examine the next higher derivatives of these variables. We find that

$$\frac{\delta[p_r]}{\delta t} = -\gamma p_1[u_{rr}] + (\gamma-1)\dot{q}r_2/v_2 = 0 \tag{97}$$

so

$$[u_{rr}] = (\gamma-1)\dot{q}_{r_2}/\gamma p_1 v_1 = \dot{q}_{r_2}/\gamma e_1 \quad , \tag{98}$$

which is negative, since $\dot{q}_{r_2}$ is negative.

The equation for $[e_r]$ is obtained as

$$\frac{\delta[e_r]}{\delta t} = -(\gamma-1)[e_r][u_{r_1} + ju_1/r_c] + \dot{q}_{r_2}/\gamma \quad , \tag{99}$$

which is of the same form as Eq. 91. It follows then, that if $[e_r] = 0$ at $t = 0$, then the sign of $[e_r]$ depends upon the sign of $\dot{q}_{r_2}$. Since the latter is negative, then $[e_r]$ is negative.

For $[v_r]$ we get

$$[v_r] = v_1[e_r]/e_1 \quad , \tag{100}$$

which is also negative.

Finally, forming

$$\frac{\delta[u_r]}{\delta t} = -[p_{rr}]v_1 - p_{r_1}[v_r] = 0 \quad , \tag{101}$$

we get

$$[p_{rr}] = -p_{r_1}[v_r]/v_1 = -p_{r_1}[e_r]/e_1 \quad , \tag{102}$$

which is negative.

These results appear in Fig. 6.

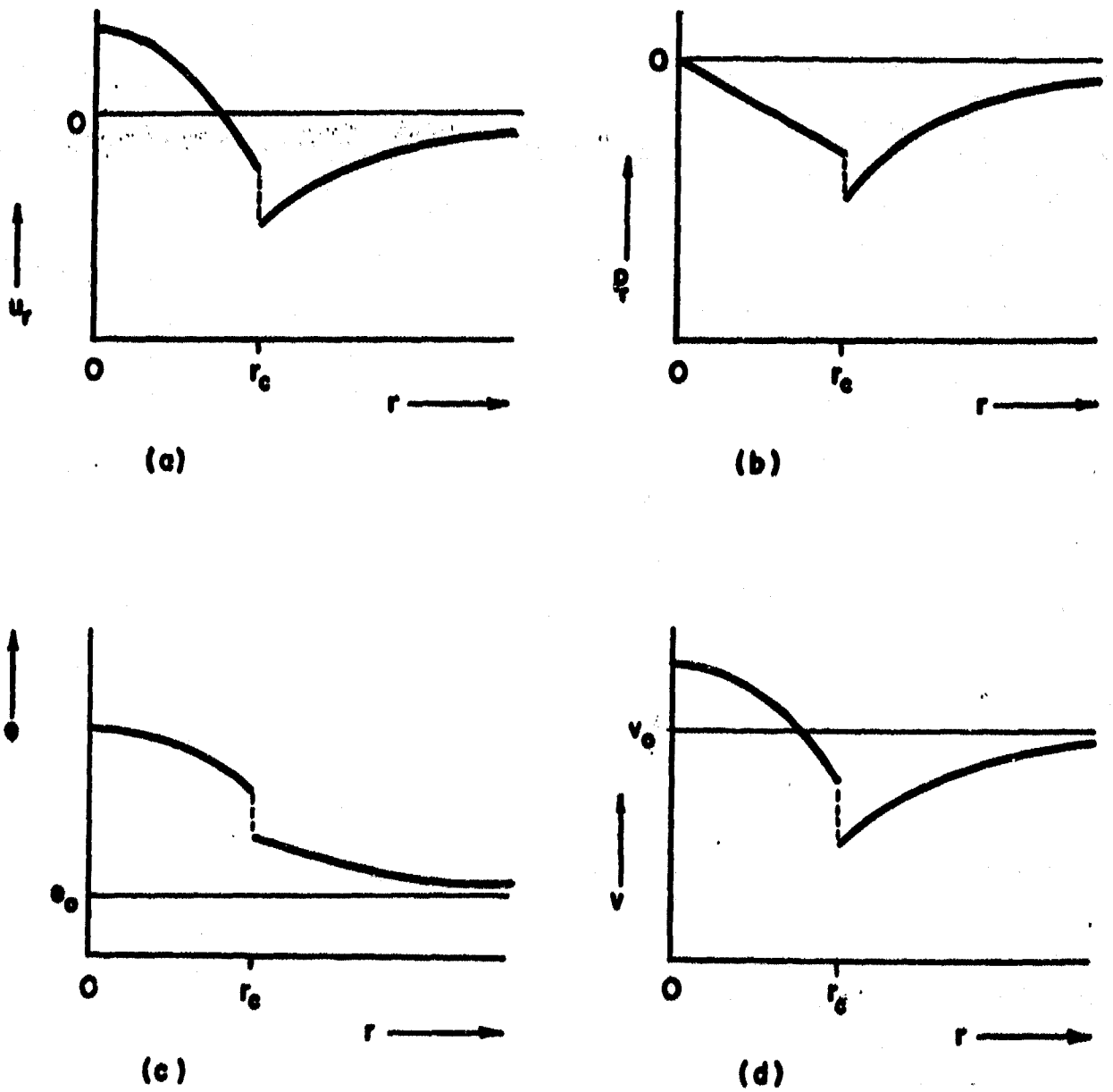

Fig. 5. Property variations as a function of radius when both q and q_r are discontinuous at the kernel edge and that edge moves along a particle path. (a) u_r vs r, (b) p_r vs r, (c) e vs r and (d) v vs r.

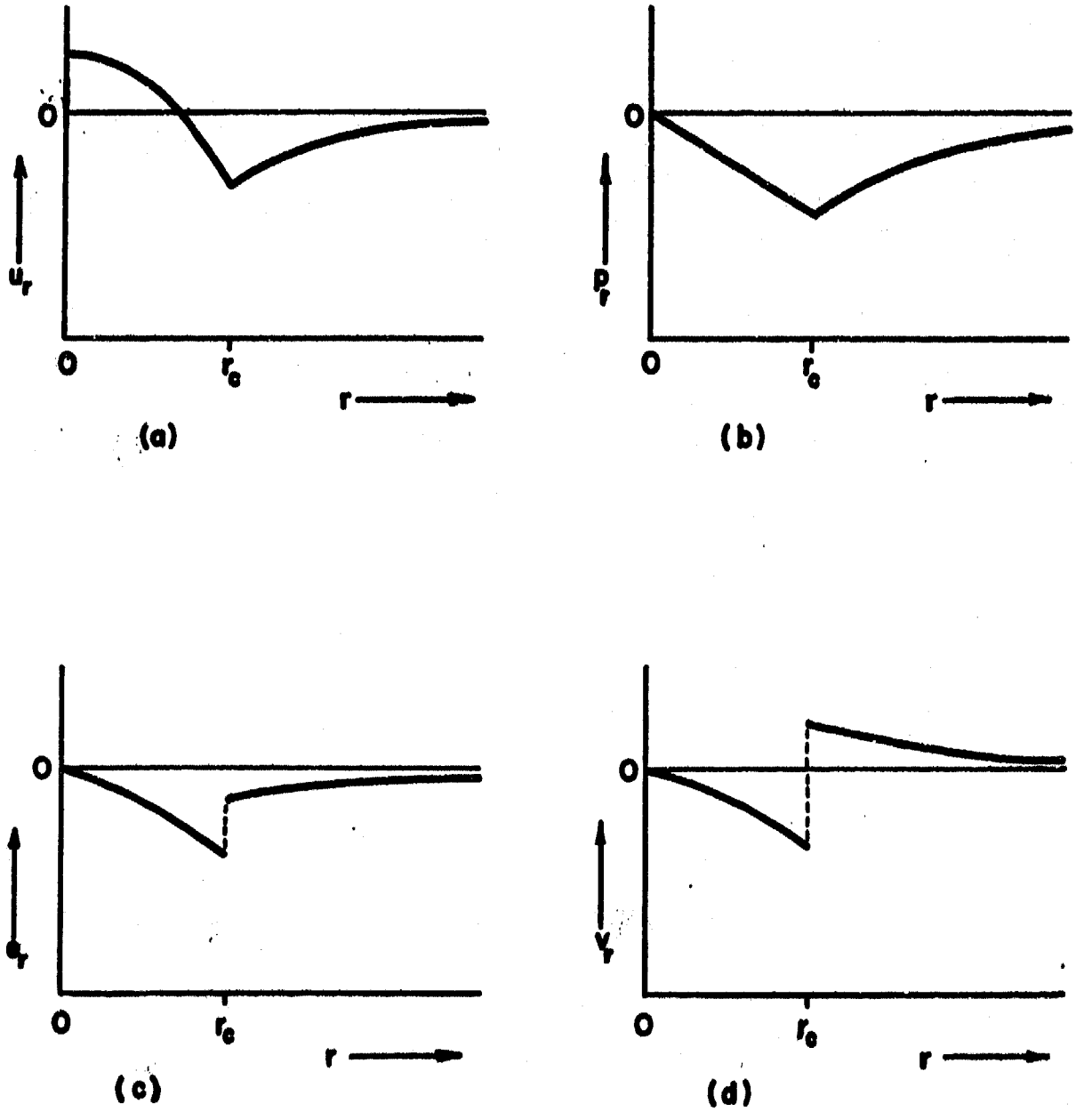

Fig. 6. Property variations as a function of radius when q is continuous but q_r is discontinuous at the kernel edge and that edge moves along a particle path. (a) u_r vs r, (b) p_r vs r, (c) e_r vs r and (d) v_r vs r.

b) Wave Surface

For $k \neq 0$, so long as there is no shock wave, u, p, v and e are continuous across r_c, with no jumps and their $\frac{\delta[\ ]}{\delta t}$ derivatives are zero.

For a $\dot{q}$ jump at r_c, from Eqs. 83, 85 and 87, we find

$$\frac{\delta[u]}{\delta t} = -v_1[p_r] - (\dot{r}_c - u_1)[u_r] = 0 \tag{103}$$

$$\frac{\delta[p]}{\delta t} = -\gamma p_2[u_r] + (\gamma-1)\dot{q}_2/v_1 - (\dot{r}_c-u_1)[p_r] = 0 \quad . \tag{104}$$

Simultaneous solution then yields

$$[u_r] = (\gamma-1)\dot{q}_2/\{a_1^2-(\dot{r}_c-u_1)^2\} = (\gamma-1)\dot{q}_2/a_1^2(1-k^2) \quad , \tag{105}$$

which is positive for $k < 1$ and negative for $k > 1$, and

$$[p_r] = (\gamma-1)k\dot{q}_2/v_1a_1(1-k^2) \quad , \tag{106}$$

which has a similar behavior.

From Eqs. 84 and 87, we find

$$\frac{\delta[e]}{\delta t} = -(\gamma-1)e_1[u_r] + \dot{q}_2 + (\dot{r}_c-u_1)[e_r] = 0 \quad , \tag{107}$$

so

$$[e_r] = -\dot{q}_2(\gamma^{-1} - k^2)/ka_1(1-k^2) \quad . \tag{108}$$

This expression is negative for $0 < k < \gamma^{-1/2}$, positive for $\gamma^{-1/2} < k < 1$ and negative for $k > 1$.

We find from differentiating Eq. 86 that

$$[v_r] = -(\gamma-1)\dot{q}_2/\gamma p_1a_1(1-k^2) \quad , \tag{109}$$

which is negative for $k < 1$ and positive for $k > 1$.

These results are shown in Fig. 7 with $k < \gamma^{-1/2}$.

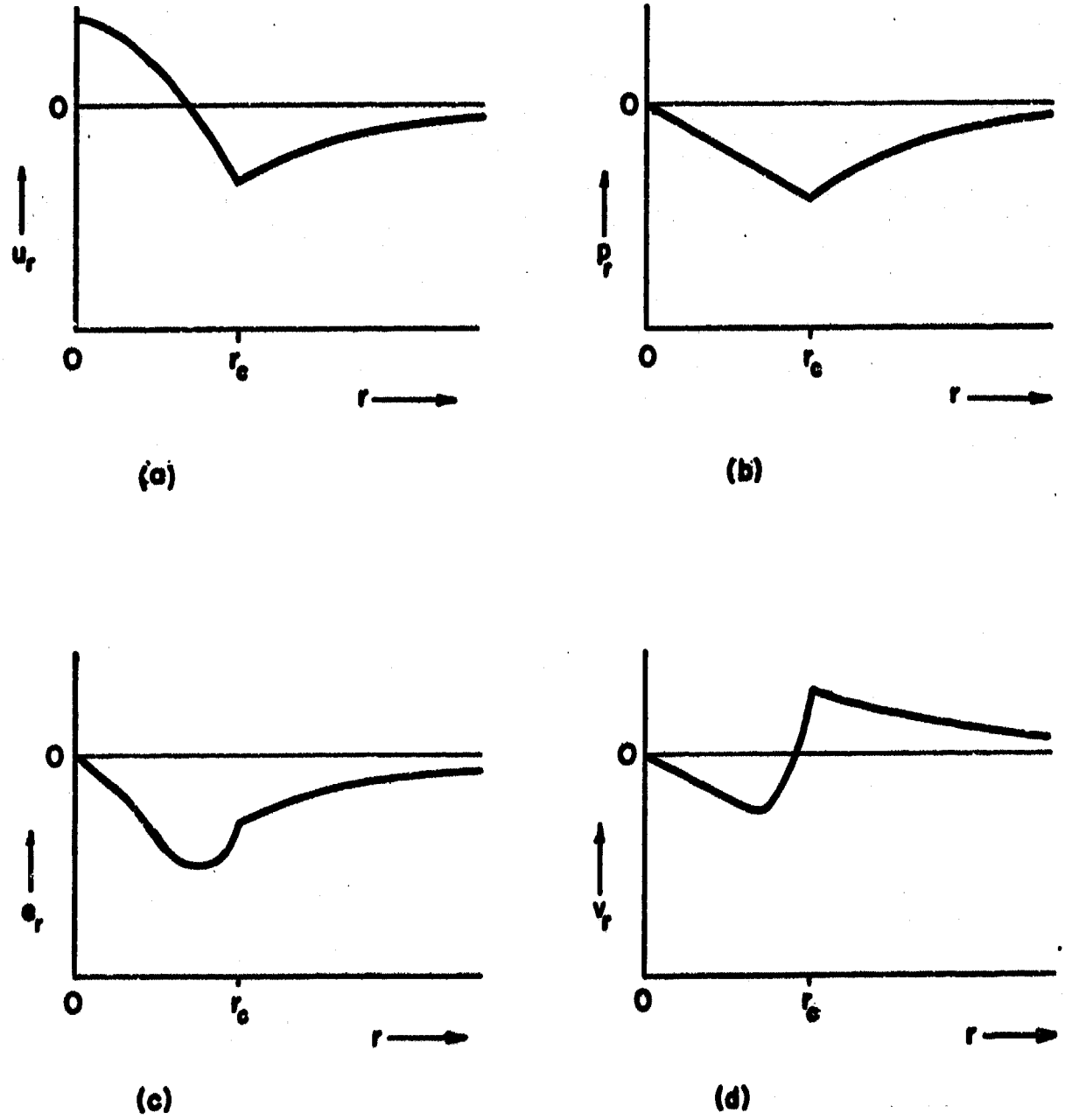

Fig. 7. Property variations as a function of radius when q is continuous but q_r is discontinuous at the kernel edge and that edge moves as a subsonic wave across particle paths with $\kappa < \gamma^{-1/2}$. (a) u_r vs r, (b) p_r vs r, (c) e_r vs r and (d) v_r vs r.

When $\dot{q}_2 = 0$ with a jump in $\dot{q}_r$ at r_c, no jumps occur in these first order spatial derivatives and we examine the second order derivatives. In this case we obtain similar forms, with

$$[u_{rr}] = (\gamma-1)\dot{q}_{r_2}/a_1^2(1-k^2) \quad , \tag{110}$$

$$[p_{rr}] = (\gamma-1)\dot{q}_{r_2}/v_1 a_1(1-k^2) \quad , \tag{111}$$

$$[e_{rr}] = -\dot{q}_{r_2}(\gamma^{-1}-k^2)/ka_1(1-k^2) \quad , \tag{112}$$

and

$$[v_{rr}] = -(\gamma-1)\dot{q}_{r_2}/\gamma k p_1 a_1(1-k^2) \quad , \tag{113}$$

whose behaviors are easily interpreted.

These results are summarized in Fig. 8 , again with $k < \gamma^{-1/2}$.

c) Shock Wave Surface

When $k > 1$ with the interface being a shock, the variables obviously jump across the shock, so the following shock equations must be satisfied

$$a_2^2 = a_1^2\left(1 + \frac{\gamma-1}{2}M^2\right)\left(\gamma M^2 - \frac{\gamma-1}{2}\right)\left(\frac{2}{\gamma+1}\right)^2/M^2 \quad , \tag{114}$$

$$p_2 = p_1\left[\frac{2\gamma}{\gamma+1}M^2 - \frac{\gamma-1}{\gamma+1}\right] \quad , \tag{115}$$

$$u_2 = u_1 + \frac{2}{\gamma+1}a_1(M - M^{-1}) \quad , \tag{116}$$

$$v_2 = \frac{2}{\gamma+1}v_1\left[\frac{\gamma-1}{2} + M^{-2}\right] \quad , \tag{117}$$

where

$$M = (\dot{r}_c - u_1)/a_1 = k \quad . \tag{118}$$

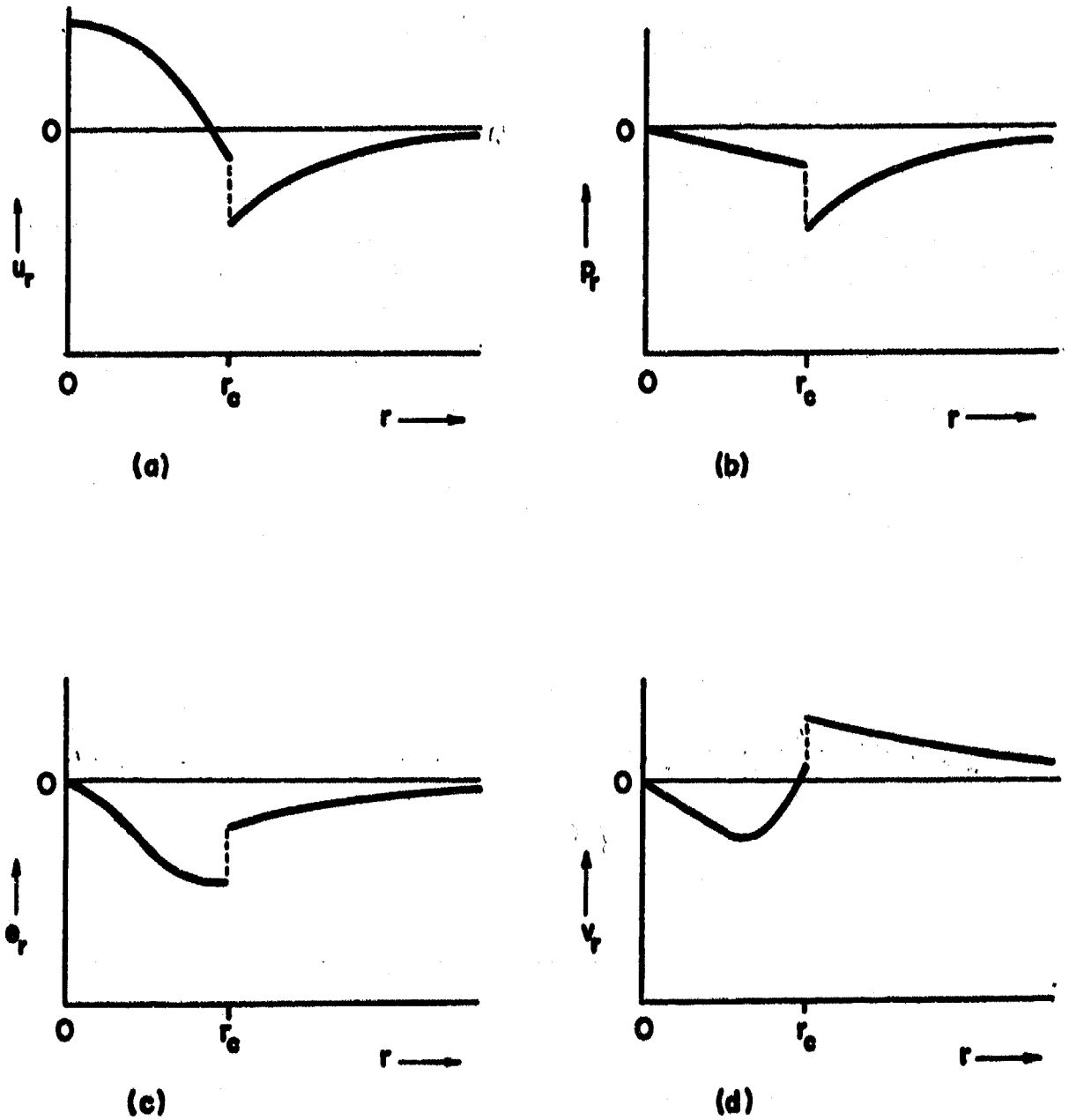

Fig. 8. Property variations as a function of radius when both q and q_r are discontinuous at the kernel edge and that edge moves as a subsonic wave across particle paths with $\kappa < \gamma^{-1/2}$. (a) u_r vs r, (b) p_r vs r, (c) e_r vs r and (d) v_r vs r.

When Eqs. 115-118 are differentiated following the shock, we obtain

$$\frac{\delta p_2}{\delta t} = \left(\frac{2\gamma}{\gamma+1} M^2 - \frac{\gamma-1}{\gamma+1}\right)\frac{\delta p_1}{\delta t} + \frac{4\gamma}{\gamma+1} p_1 M \frac{\delta M}{\delta t} \quad , \tag{119}$$

$$\frac{\delta u_2}{\delta t} = \frac{\delta u_1}{\delta t} + \frac{2}{\gamma+1}(M-M^{-1})\frac{\delta a_1}{\delta t} + (1+M^{-2})\, a_1 \frac{\delta M}{\delta t} \quad , \tag{120}$$

$$\frac{\delta v_2}{\delta t} = \frac{2}{\gamma+1}\left\{\left(\frac{\gamma-1}{2} + M^{-2}\right)\frac{\delta v_1}{\delta t} - 2v_1 M^{-3}\frac{\delta M}{\delta t}\right\} \quad , \tag{121}$$

and

$$\frac{\delta M}{\delta t} = \left(\ddot{r}_c - \frac{\delta u_1}{\delta t}\right)/a_1 - (\dot{r}_c - u_1)a_1^{-2}\frac{\delta a_1}{\delta t} \quad , \tag{122}$$

where

$$\frac{\delta p_1}{\delta t} = -\gamma p_1(u_{r_1} + ju_1/r_c) + (\dot{r}_c - u_1)p_{r_1} \quad , \tag{123}$$

$$\frac{\delta u_1}{\delta t} = -v_1 p_{r_1} + (\dot{r}_c - u_1)u_{r_1} \quad , \tag{124}$$

$$\frac{\delta v_1}{\delta t} = v_1(u_{r_1} - ju_1/r_c) + (\dot{r}_c - u_1)v_{r_1} \quad , \tag{125}$$

$$\frac{\delta a_1}{\delta t} = -\frac{(\gamma-1)}{2} a_1(u_{r_1} + ju_1/r_c) + (\dot{r}_c - u_1)a_{r_1} \tag{126}$$

$$\frac{\delta p_2}{\delta t} = -\gamma p_2(u_{r_2} + ju_2/r_c) + (\gamma-1)q_2/v_2 + (\dot{r}_c - u_2)p_{r_2} \quad , \tag{127}$$

$$\frac{\delta u_2}{\delta t} = -v_2 p_{r_2} + (\dot{r}_c - u_2)u_{r_2} \quad , \tag{128}$$

$$\frac{\delta v_2}{\delta t} = v_2(u_{r_2} + ju_2/r_c) + (\dot{r}_c - u_2)v_{r_2} \quad . \tag{129}$$

Solving Eqs. 127 and 128 for u_{r_2} and p_{r_2}, we obtain

$$u_{r_2} = \left\{(\dot{r}_c - u_2)\frac{\delta u_2}{\delta t} + v_2\frac{\delta p_2}{\delta t} - (\gamma-1)q_2 + a_2^2 j u_2/r_c\right\}/\{(\dot{r}_c-u_2)^2 - a_2\} \qquad (130)$$

and

$$p_{r_2} = \left\{(\dot{r}_c-u_2)\left[\frac{\delta p_2}{\delta t} - (\gamma-1)\dot{q}_2/v_2 + \gamma p_2 j u_2/r_c\right] + \gamma p_2\frac{\delta u_2}{\delta t}\right\}/\left\{(\dot{r}_c-u_2)^2 - a_2^2\right\} . \qquad (131)$$

From Eqs. 129 and 86, we obtain

$$v_{r_2} = \left\{\frac{\delta v_2}{\delta t} - v_2(u_{r_2} + j u_2/r_c)\right\}/\{\dot{r}_c - u_2\} \quad , \qquad (132)$$

and

$$e_{r_2} = (p_2 v_{r_2} + v_2 p_{r_2})/(\gamma-1) \quad . \qquad (133)$$

It should be noted that Eqs. 130-133 can be expressed in terms of (1) $\dot{q}_2$, (2) r_c and its time derivatives and (3) the flow variables and their spatial derivatives evaluated just ahead of the shock. However, the resulting expressions are quite long, so have not been included here.

The explicit method of integration in the CLOUD program does not properly handle the jumps and corners in the variables which result from discontinuities in $\dot{q}$ or $\dot{q}_r$ at the kernel edge. As a consequence, the computation becomes unstable and soon "blows up." However, if $\dot{q}$ is sufficiently smooth, with both $\dot{q}$ and $\dot{q}_r$ equal to zero at the kernel edge, these jumps and corners disappear. Then CLOUD seems to work very nicely so long as reaction may be neglected.

7.11 Status at the End of Grant Period

Calculations for several time lines beyond the initial time line from the CLOUD program have been made, assuming in the implicit program that integration along the particle direction as well as along the K^+ and K^- directions can be adequately represented by the arithmetic average of values for the two end points. Examination of the computed values for u_r and p_r near the origin indicated that these variables did not seem to be behaving properly. The reason appears to be that for the K^+ and K^- directions the previous integration assumption is inadequate, as we will now show.

Let us consider the integral of $\frac{\delta K_r^-}{\delta t} = u - K^- a$ near the origin. The behavior of u vs r for time lines t_n and t_{n+1} are approximately as shown in Fig. 9. If we use average values corresponding to the end points, we get

$$r(1,n+1) - r(2,n) = \left\{\frac{[u(1,n+1)+u(2,n)]}{2} - K^- \frac{[a(1,n+1)+a(2,n)]}{2}\right\}[t_{n+1}-t_n] \quad . \qquad (134)$$

However, $u(1,n+1) = u(1,n) = 0$, so the contribution from u is $\frac{u(2,n)}{2}(t_{n+1}-t_n)$, which is simply the average value of u multiplied by the time increment. Next, we consider the dashed line which approximates the path. Clearly, the integral of u along this path is greater than $\frac{u(2,n)}{2}(t_{n+1}-t_n)$, so we require a better approximation to u.

We obtain a better approximation if we assume u may be represented by a function containing two groups of terms. The first group represents how u varies along the $t = t_n$ line; the second group represents how much u has changed in time $(t - t_n)$ from its value at t_n. Thus we write

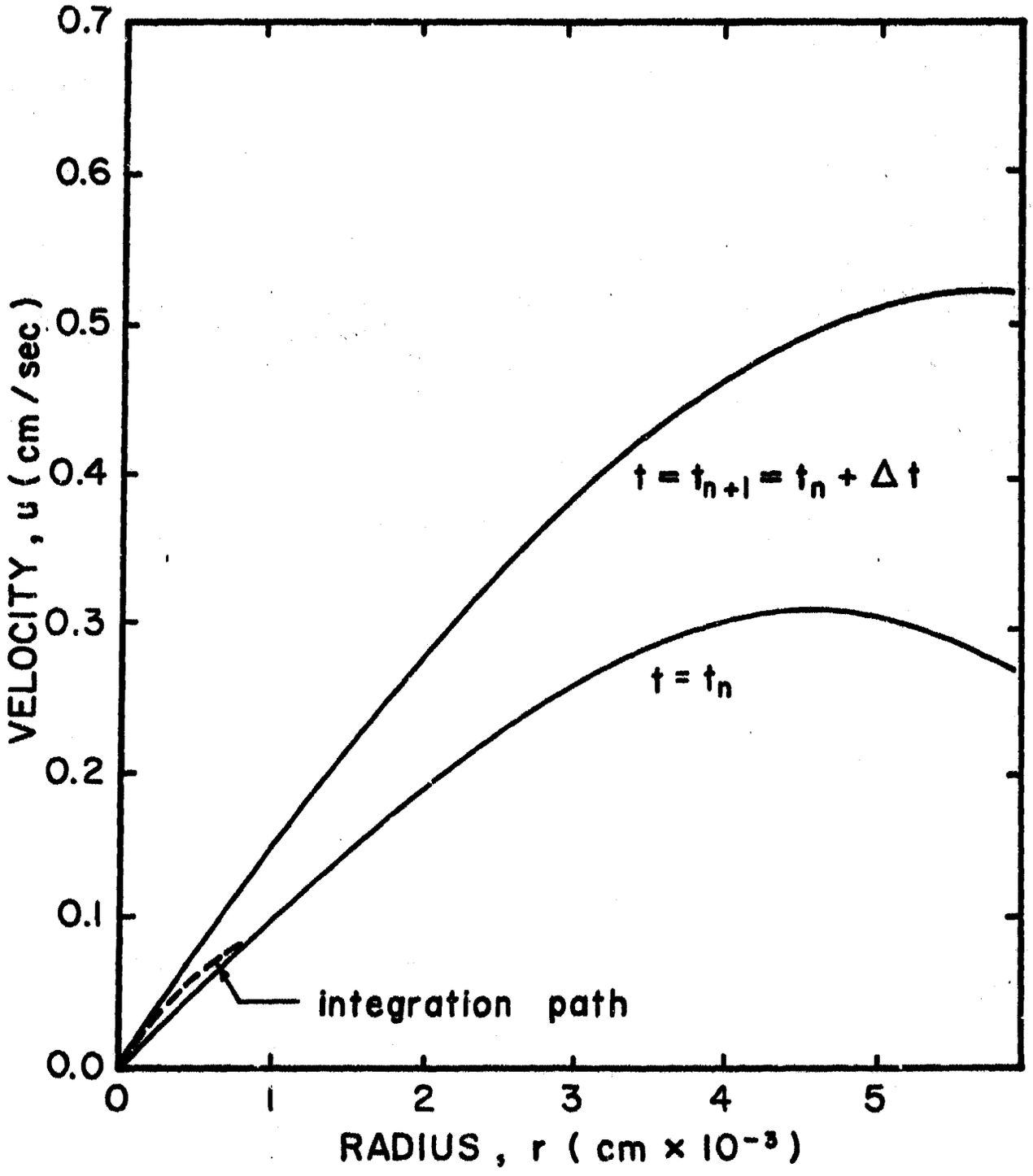

Fig. 9. Behavior of particle velocity versus radius near the origin for times t_n and t_{n+1}.

$$u = u(1,n) + u_r(1,n)[r-r(1,n)] + u_{rr}(1,n)\frac{[r-r(1,n)]^2}{2}$$

$$+ \left\{\dot{u}(1,n) + \dot{u}_r(1,n)[r-r(1,n)] + \dot{u}_{rr}(1,n)\frac{[r-r(1,n)]^2}{2}\right\}[t-t_n] \quad , \quad (135)$$

where $\dot{u} = \frac{Du}{Dt}$ and $r-r(1,n)$ is given to first order in t by

$$r-r(1,n) = \frac{-[r(2,n) - r(1,n)]}{t_{n+1} - t_n}[t-t_{n+1}] \quad . \quad (136)$$

Expressions similar to $\underline{u}$ can be written for a or for other variables when integrating $\frac{\delta^{K^-}\underline{u}}{\delta t}$ and $\frac{\delta^{K^-}p}{\delta t}$. A similar concept can be applied when integrating in the K^+ direction. Changes in the computer program to incorporate these concepts were underway at the end of the grant period.

A second conversion also was underway, for the University computing facility was in transition from an IBM 360 system to a CDC system. The switch to a different machine requires conversions of programs written specifically for IBM machines.

As this account has tried to indicate, difficulties have arisen during the period of the grant. Generally we have been able to identify the cause, to analyze why it has given us difficulty and to devise a method to overcome each difficulty. In conclusion, while we have not yet developed a computer program which successfully used an implicit technique to solve our problem, we still believe our approach can succeed and intend to pursue the matter further.

VIII DIRECT INITIATION OF DETONATION BY NON-IDEAL BLAST WAVES

This work is fully described in AFOSR TR-77-0842. Therefore, only a brief description of the work will be given here. The reader is referred to the full report for more detailed description.

The purpose of this study was to examine the process of direct initiation for a non-ideal blast wave source for reasonably realistic kinetics in the gas phase region surrounding the source. The kinetics was modeled as Arrhenius kinetics for the hydrogen-oxygen reaction but it was assumed that the ignition delay time was infinite outside the temperature range of 1000 K to 2700 K. This is a reasonably realistic model of the actual kinetics because below 1000 K the delay to explosion increases very rapidly with dropping temperature while above about 2700 K the combustion reaction in the hydrogen-oxygen system becomes endothermic because of the excessive amount of dissociation produced by the high temperature. Thus, in the hydrogen-oxygen system one would expect to see an explosion induced in the high temperature gas only over the range of about 1000 to 2700 K.

The calculations were performed as follows. Existing CLOUD output for various cases of bursting spheres and ramp addition of energy plus a number of new calculations for specific cases were used to describe the blast wave flow from a typical non-ideal source (either a bursting sphere or a region where the energy is added as a ramp addition of energy). This last addition quite closely approximates spark addition of energy. These background flows were all calculated in dimensionless coordinates. Thus multiplication by the proper dimensional quantities allows one to change the actual size of the source region without recalculating the entire flow field. A

program was constructed which examined the time, temperature and pressure history of cells number 52 through 130 for these different runs. In each case, along each Lagrangian cell, which represents a particle path, hydrogen-oxygen kinetics was assumed and the accumulated delay to explosion was calculated using an experimentally determined Arrhenius equation for the delay. In one or more of these cells the accumulated delay to explosion had a minimum time and this was assumed to be the point in the spherical cell surrounding the blast source which first exploded. The calculated dimensionless time to explosion was converted to a real time fractional delay to explosion by using the size of the blast source as a scaling parameter. As the source gets smaller for any fixed energy density source the total energy in the source gets smaller and at the same time the real accumulated fractional explosion delay time gets smaller eventually reaching a value of one. Under these circumstances a smaller sized source will not produce direct initiation of detonation. Thus, one can systematically study the effect of energy addition rates and of energy density as well as total energy of the source region on the initiation behavior for an hydrogen-oxygen detonation system. This was done and the results show that for sources with low energy density the source energy required to produce detonation rises to infinity while for high energy density there is an asymptotic minimum value of source energy which is required for initiation. This behavior agrees quite well with the recent description of initiation that has been presented by Professor John Lee of McGill University. Even though this study showed ignition delay times and initiation energies which were well below what one finds experimentally for this type of source behavior the trends are qualitatively correct. The large quantitative difference (our energies are approximately a

factor of 100 lower than the experimental energies) can be related to the fact that direct initiation only occurs when there is sufficient time to produce transverse waves of sufficient amplitude to cause self-sustenance of the wave. The simple theory in the report, however, predicts the time at which direct homogeneous initiation would occur and has nothing to say about the development of transverse wave structure.

IX OTHER WORK OF INTEREST

There has been a considerable amount of effort expended over the period of the grant to study the effect of source behavior on the nature of the blast wave produced when the source is a low energy density source similar to that which occurs in a vapor cloud explosion or in the explosion of an FAE device. Briefly, systematic studies have been performed for blast waves produced by bursting spheres, by the ramp addition of energy (which models a spark) and by constant velocity and accelerating flames from very low Mach numbers up to Mach numbers above the Chapman-Jouguet Mach number. As a result of these studies the behavior of the blast wave from bursting spheres and from constant velocity flames can now be estimated quite accurately if either the initial conditions of the bursting sphere are known or if the combustion system and the flame velocity are known for the constant velocity flame case. Additionally, it has been shown that a spherical accelerating flame will not produce overpressures in excess of that produced by the highest flame velocity in the system when the explosion consists of a flame traveling at that high velocity. This means that calculations for constant velocity flames are adequate to estimate blast damage if the maximum flame velocity is known. This work has lead to one M.S. and two Ph.D. theses and

to four papers, two of which have been published and two of which have been submitted to journals for publication (15,18-23). Additionally, two M.S. theses are currently in the process of preparation. These will cover the experimental work on initiation delay times for propylene oxide-nitrogen-oxygen mixtures and the effect of inhibitors and promoters on ignition delay times for propane-air mixtures.

REFERENCES

1. Strehlow, R. A., "Gas Phase Detonations: Recent Developments," Combustion and Flame 12, 81-101 (1968).

2. Erpenbeck, J. J., Phys. Fluids 7, 684 (1964); 8, 1192 (1965); 9, 1293 (1966). Strehlow, R. A. and Fernandes, F. D., Combustion and Flame 9, 109 (1965).

3. Strehlow, R. A., Astronautica Acta 14, 539-548 (1969).

4. Strehlow, R. A., Astonautica Acta 15, 345-357 (1970).

5. Strehlow, R. A., Maurer, R. E., and Rajan, S., AIAA Journal 7, 323 (1969); Strehlow, R. A. and Engel, C. D., AIAA Journal 7, 492 (1969).

6. Strehlow, R. A. and Biller, J. R., Combustion and Flame 13, 577-582 (1969).

7. Barthel, H. O., Phys. Fluids 15, 43 (1972).

8. Barthel, H. O., Phys. Fluids 17, 1547 (1974).

9. Taylor, G. I., Proc. Roy. Soc. A201, 159-174 (1950).

10. Bach, G. G., Krystantas, R., and Lee, J. H., "Initiation Criterion for Developing Gaseous Detonations," 13th Symposium (International) on Combustion (The Combustion Institute, Pittsburgh, 1971), pp. 1097-1110.

11. Delaney, R. D., "An investigation of the chemical-gasdynamic interaction for isomers of ethylene oxide and propylene oxide," M.S. thesis, Aeronautical and Astronautical Engineering Department, University of Illinois (1975).

12. Milne, C. A., Philos. Mag. 42, 96 (1921).

13. Bailey, H. E., Phys. Fluids 11, 2292 (1969).

14. Savage, L. D., private communication.

15. Adamczyk, A. A., "An investigation of blast waves generated from non-ideal energy sources," Ph.D. thesis, Aeronautical and Astronautical Engineering Department, University of Illinois (November 1976).

16. Barthel, H. O., submitted to Astronautica Acta (1977).

17. Cesarone, R. J., "Direct initiation of detonation by non-ideal blast waves," M.S. thesis, Aeronautical and Astronautical Engineering Department, University of Illinois (June 1977); also, AAE Technical Report 77-4, UILU-Eng 77 0504, AFOSR-TR-77-0842.

18. Ricker, R. E., "Blast waves from bursting pressurized spheres," M.S. thesis, Aeronautical and Astronautical Engineering Department, University of Illinois (1975).

19. Strehlow, R. A. and R. E. Ricker, "The Blast Wave from a Bursting Sphere," AIChE Loss Prevention 10, 115-121 (1976).

20. Strehlow, R. A., "Non_ideal Explosions, the Blast Wave from Low Energy Density Explosion Sources," Minutes of the 17th Explosives Safety Seminar, Denver, Colorado, September 1976, pp. 1721-1742.

21. Luckritz, R. T., "An investigation of blast waves generated by constant velocity flames," Ph.D. thesis, Department of Chemical Engineering, University of Maryland (March 1977); also, AAE TR-77-2, UILU-Eng 77 0502.

22. Strehlow, R. A. and R. T. Luckritz, "On the Blast Wave Produced by Constant Velocity Combustion Waves, AAE TR-77-3, UILU-Eng 77 0503. Submitted to Acta Astronautica, April 1977.

23. Strehlow, R. A., R. T. Luckritz, A. A. Adamczyk, and S. Shimpi, "The Blast Wave Generated by Constant Velocity Flames," AAE TR-77-9, UILU-Eng 77 0509. Submitted to Combustion and Flame, July 1977.